Scholar Commons
USF University of South Florida

University of South Florida
Scholar Commons

Graduate Theses and Dissertations | Graduate School

1-1-2014

Fabrication and Characterization of Magnetic Nanostructures

Kevin Scott
University of South Florida, kscott@mail.usf.edu

Follow this and additional works at: http://scholarcommons.usf.edu/etd

 Part of the Nanotechnology Fabrication Commons

Scholar Commons Citation
Scott, Kevin, "Fabrication and Characterization of Magnetic Nanostructures" (2014). *Graduate Theses and Dissertations.*
http://scholarcommons.usf.edu/etd/5437

This Thesis is brought to you for free and open access by the Graduate School at Scholar Commons. It has been accepted for inclusion in Graduate Theses and Dissertations by an authorized administrator of Scholar Commons. For more information, please contact scholarcommons@usf.edu.

Fabrication and Characterization of Magnetic Nanostructures

by

Kevin Scott

A thesis submitted in partial fulfillment
of the requirements for the degree of
Master of Science in Electrical Engineering
Department of Electrical Engineering
College of Engineering
University of South Florida

Major Professor: Sanjukta Bhanja, Ph.D.
Michael Celestin, Ph.D.
Al-Aakhir Rogers, Ph.D.

Date of Approval:
October 30, 2014

Keywords: Nanomagnets, Electron-Beam Lithography, SEM, MFM, Nanotechnology

Copyright © 2014, Kevin Scott

Table of Contents

List of Tables

List of Figures

Abstract

Magnetic permalloy nanostructures were fabricated onto a silicon wafer using electron beam lithography and a liftoff process. The lithography was performed with a Hitachi SU-70 SEM retrofitted with a Nabity NPGS lithography conversion kit. PMMA of 950kDa molecular weight was used as the photoresist. Features were either nanowires, nanodots, or elliptical or rectangular nanostructures. The nanowires had dimensions of 15µm x 200nm x 40nm, the nanodots had diameters of 145nm and thickness of 12nm, and the ellipses and rectangles had dimensions of 110nm x 50nm x 13nm. Characterization of the nanostructures was performed using the same Hitachi SEM as well as a Digital Instruments DI 3100 Nanoscope IIIa AFM used in magnetic force imaging mode. The SEM was used to measure lateral dimensions of the features and to capture images of features for proper documentation and for external simulation studies. The MFM was used to capture magnetic images of the samples to determine the magnetic state of the nanowires or arrays.

Chapter 1: Introduction

The study of nanomagnetic devices for data storage, transmission, and computation has been well analyzed [1-5]. Integrating magnetic nanostructures into system hardware can improve quality and performance of the system due to the low power consumption, non-volatility of information, radiation-hardened nature, and simple architectural layout of the nanomagnets [7]. Nanomagnets with a pair of low-energy states due to magnetic anisotropy can store binary data and perform Boolean functions [8]. Nanomagnets with many low-energy states due to circular symmetry can be used as high sensitivity magnetic field sensors [7] and novel computer image processing [9].

The work presented in this thesis involves the implementation of magnetic nanostructures in various samples. Designs or design parameters were determined externally and then given to me. My role within the research group was to fabricate and characterize the samples and then export my results to other members of the group for analysis and interpretation. This thesis, therefore, will only cover the fabrication and characterization of the samples. A chapter will be devoted to relevant background information of the fabrication and characterization methods utilized. A short chapter will then offer an introduction to the theory of the three samples analyzed in this thesis. The brunt of the work presented will then describe the fabrication process and the characterization results.

Chapter 2: Background and Theory

2.1 Scanning Electron Microscope

An SEM (scanning electron microscope) is a microscope that scans a focused beam of electrons over a sample surface as a means of generating an image. The small diameter of this beam (1-50nm) allows features unresolvable by an optical microscope to be clearly observed. This is due to the effective wavelength of the electron being smaller than the wavelength of visible light.

A cross-sectional view of an SEM is shown in figure 2.1 [6]. The electron beam, also referred to as the primary beam, is shown in red and all of the main components are identified.

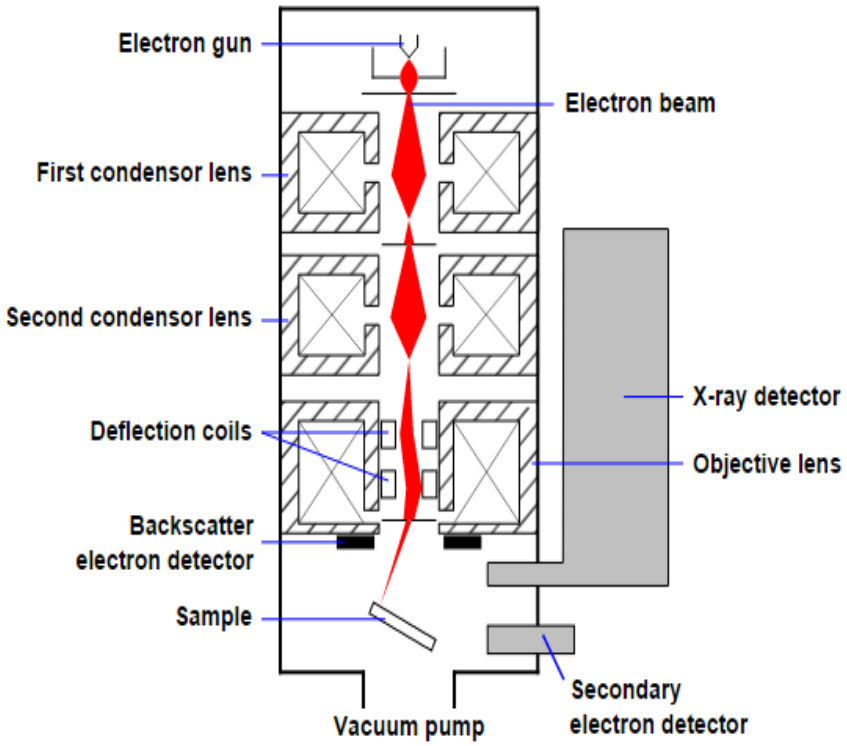

Figure 2.1: A cross-sectional schematic of an SEM [6].

The primary beam originates from the electron gun, or electron source. A cross-sectional view of a generic electron source is shown in figure 2.2. Electrons are emitted from the tip and a voltage is applied to Anode 2 to accelerate the electrons down the column. This accelerating voltage is user selected referred typically assumes a value between 0.5-30kV. The electrons can be emitted from the tip either through thermal emission, field emission, or both. Thermal emission sources apply a large bias across the tip to heat the tip. This heat energy allows the electrons to overcome the work function of the source and emit in a spray pattern. This spray is focused by the electrostatic lens created by applying a negative bias to Electrode 1. Field emission sources apply a positive bias to Electrode 1 to extract electrons from the tip. Field emission tips are not heated and for this reason are often referred to as cold emission sources. A Schottky-type source effectively combines these two by acting as a thermally-assisted field emission source. Thermionic sources are desirable for their low vacuum operating requirements and their stable emission current. Field emission sources are desirable for their large current densities and small beam diameters. Schottky-type sources are desirable for their small beam diameters and their large and stable emission currents [10, 11].

The beam then travels down the column and is focused to a small point through a series of apertures and magnetic lenses. An aperture is a sheet of metal with a small hole punched out.

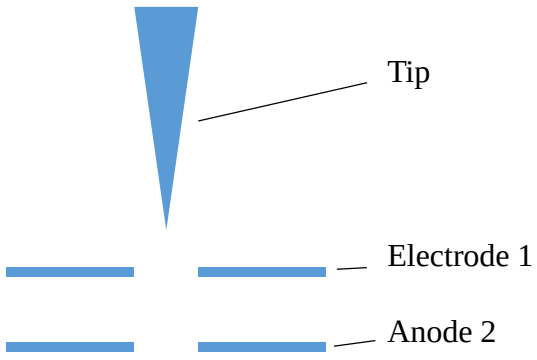

Figure 2.2: Generic cross-sectional view of an SEM electron source.

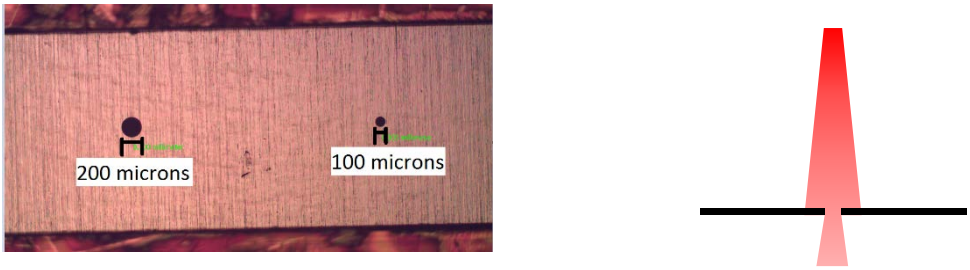

(a) (b)

Figure 2.3: SEM column apertures. (a) Shows an actual adjustable aperture plate with four apertures. (b) Shows an illustration of an aperture acting on the primary beam.

The diameter of this hole can vary from 50-200µm. The apertures can be either adjustable or stationary and serve to physically block electrons outside of a specific primary beam radius from continuing down the column. Figure 2.3 shows an actual adjustable aperture plate with four apertures punched out, as well as an illustration of the function of an aperture.

A magnetic lens is formed by encasing a solenoid with a ferromagnetic material. All of the magnetic field lines produced by the solenoid are concentrated through an airgap in the interior of the casing and a magnetic lens is formed. The primary beam converges upon passing through this lens, and then diverges. The position of the primary beam focal point shifts

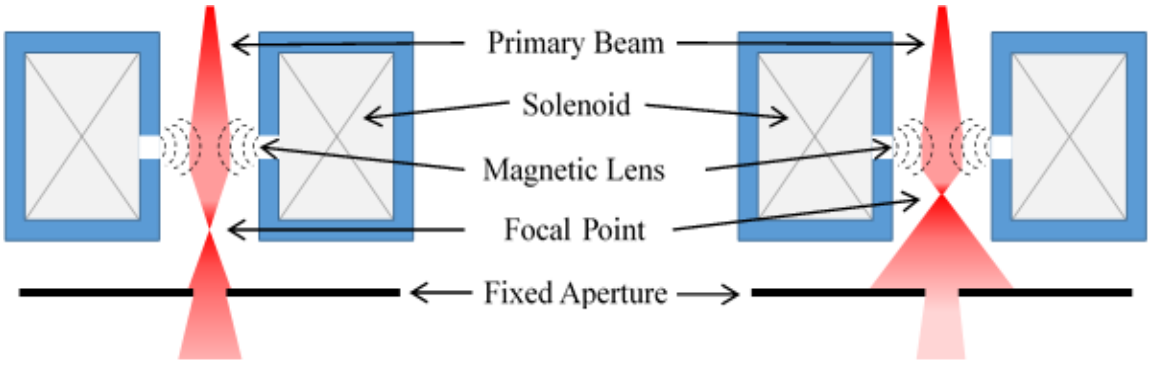

(a) (b)

Figure 2.4: Condenser lens assembly. (a) A weak magnetic lens causes a low focal point and a focused beam to be incident onto the fixed aperture. A large primary current therefore passes through and continues down the column. (b) Shows a strong magnetic lens causing a high focal point and defocused beam to be incident onto the fixed aperture. A smaller primary current therefore passes through and continues down the column.

according to the strength of the magnetic lens. The condenser lens and the objective lens of the SEM both function in this manner but perform different applications.

The condenser lens is used to control the current of the primary beam and subsequently the spot size of the primary beam, or the diameter of the primary beam upon impacting the sample. Figure 2.4 shows a cross-sectional view of a condenser lens assembly. A stationary aperture is positioned at a fixed distance below the condenser lens and the primary beam is projected onto this aperture. As the magnetic lens is weakened, many primary electrons are able to pass through the aperture. As the magnetic lens is strengthened, the primary beam is defocused and the effective electron density of the primary beam is decreased. This causes fewer primary electrons to pass through the aperture. The primary beam then continues to the objective lens where it is focused onto the sample. The strength of the objective magnetic lens mostly determines the primary beam focal point position, but also has a slight effect on the primary beam spot size. The greater effect on spot size, however, is the primary beam current incident on the objective lens, and this why the condenser lens plays a large role on the spot size. The smallest spot size is achieved from a high energy, low current primary beam.

The primary beam passes through a pair of scan coils between the condenser lens and the objective lens. These scan coils serve to scan the beam in the raster pattern shown in figure 2.5

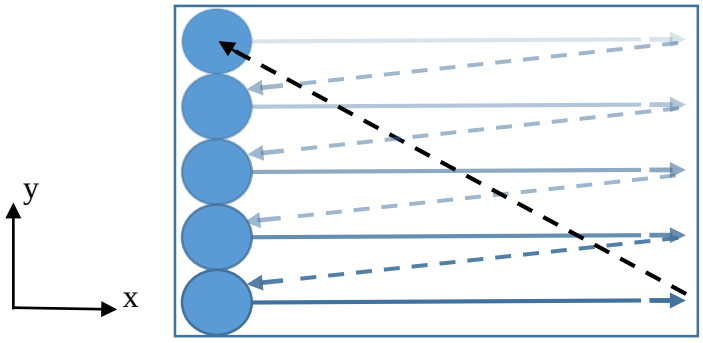

Figure 2.5: Raster pattern of the SEM primary beam. The fast scan axis corresponds to the x-axis and the slow scan axis corresponds to the y-axis.

across the surface of the sample. This raster pattern is generated by a pair of sawtooth signals applied to the scan coils. The fast scan axis has a higher-frequency signal applied to its scan coil than the slow scan axis.

As the primary beam impacts and penetrates the sample, it scatters according to the excitation volume shown in figure 2.6 [12, 13]. This pattern is generated as a result of forward scattering and backscattering of the primary electrons. Forward scattering is the slight expansion

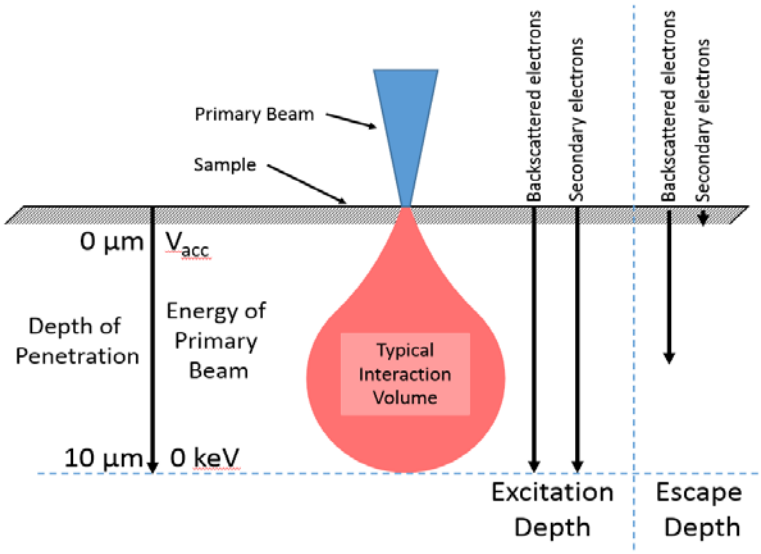

Figure 2.6: Typical interaction volume the primary beam inside the sample. The relative excitation and escape depths are shown along with the expected depth of primary beam penetration.

of the primary beam as a result of the primary electrons colliding with sample-bound electrons. Backscattering is a significant change in trajectory of the primary electrons as a result of direct collisions with the more-massive sample-bound nuclei. Primary electrons can typically travel up to 10µm inside the sample, and since backscattered electrons are simply redirected primary electrons, the excitation volume maintains a spherical teardrop shape [14]. The sample-bound electrons excited during forward scattering events are referred to as secondary electrons and each absorb approximately 5-50eV [15] of energy from the primary electrons and scatter within the

sample. The secondary electrons located within 30nm of the sample surface are able to escape the sample if they scatter in the direction of the surface.

A secondary electron detector detects the amount of emitted secondary electrons as a function of primary beam position. A raised edge on the sample provides a larger surface area for these secondary electrons to escape from and a recessed area in the sample provides a smaller surface area for these secondary electrons to escape from. A secondary electron image is a compilation of points whose positions are relative to the position of the primary beam on the sample and whose brightness are determined by the relative quantity of secondary electrons emitted from that respective primary beam dwell point.

2.2 Electron-Beam Lithography

Lithography is the process of physically printing features from one medium to another. Electron-beam lithography utilizes the primary beam of the SEM to transfer a computer-generated pattern to a photoresist-coated substrate. The pattern is created as an array of shapes and converted by the SEM to a series of dwell points. The scan coil signal is modified to

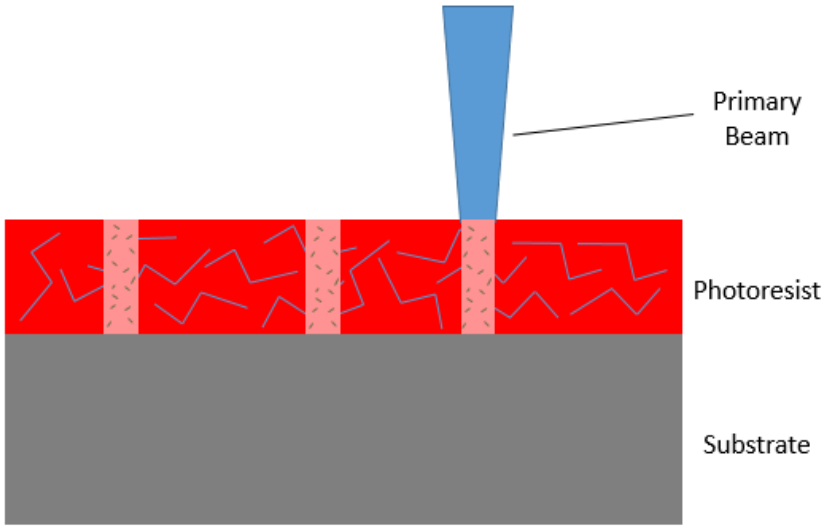

Figure 2.7: The primary beam exposing the photoresist and performing chain scission on the long polymer chains.

accommodate only these dwell points and the primary beam is forced to perform a single scan according to this pattern. In this manner, the beam transfers the pattern to the photoresist.

The photoresist used throughout this thesis was a positive-tone resist. This means that the resist consisted of long molecular chains of a polymer which would break into smaller chains when irradiated by the primary beam. This process is known as chain scission and is depiced in figure 2.7. These smaller chains would expectedly maintain a lower molecular weight and higher solubility than the longer polymer chains.

Pattern features are written by the beam in a serpentine manner according to specific parameters input by the user. Figure 2.8 shows the serpentine write pattern and labels some parameters used to expose the photoresist. The dwell time is the length of time the primary beam spends at each exposure point and is typically in the order of microseconds. The center-to-center distance (CCD) is the distance between adjacent exposure points of the same row, and the line spacing (LS) is the distance between adjacent exposure points of the same column. Both parameters are tyipcally in the order of nanometers. The exposure dose is the measure of the

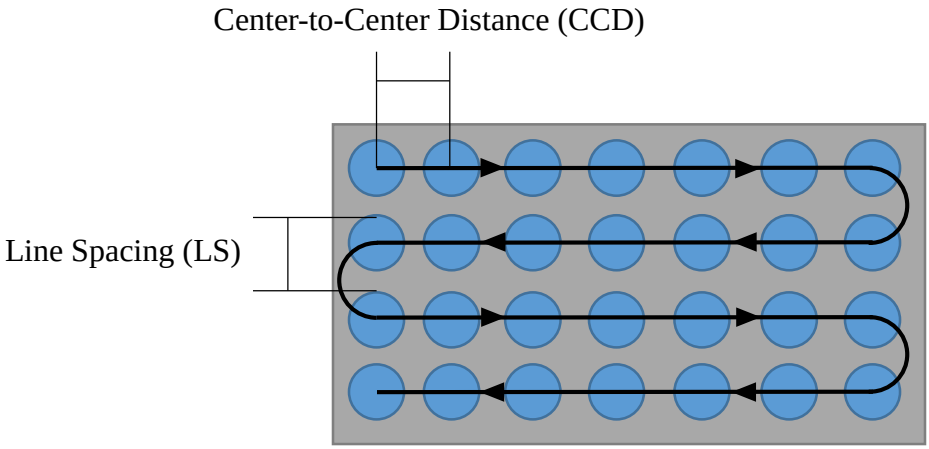

Figure 2.8: The primary beam exposes shapes in a serpentine manner. The distance between adjacent exposure points of the same row is called the center-to-center distance, or CCD. The distance between adjacent exposure points in the same column is called the line spacing, or LS.

energy transferred by the primary beam to the photoresist per unit area and is typically in the order of hundreds of microcoulombs per square centimeter. The primary beam current is measured and is tyipcally on the order of picoamperes. If all parameters are converted to the same magnitude then the total write time for a pattern is given by equation 2.1

$$T = \frac{DA}{I} \tag{2.1}$$

where T equals total write-time, D equals exposure dose, A equals exposure area, and I equals primary beam current [16].

Each exposure point generates the excitation volume shown in figure 2.6. A more detailed excitation volume is shown in figures 2.9 and 2.10 through Monte Carlo simulations [17]. The sample in these simulations is modeled after the samples used in this thesis.

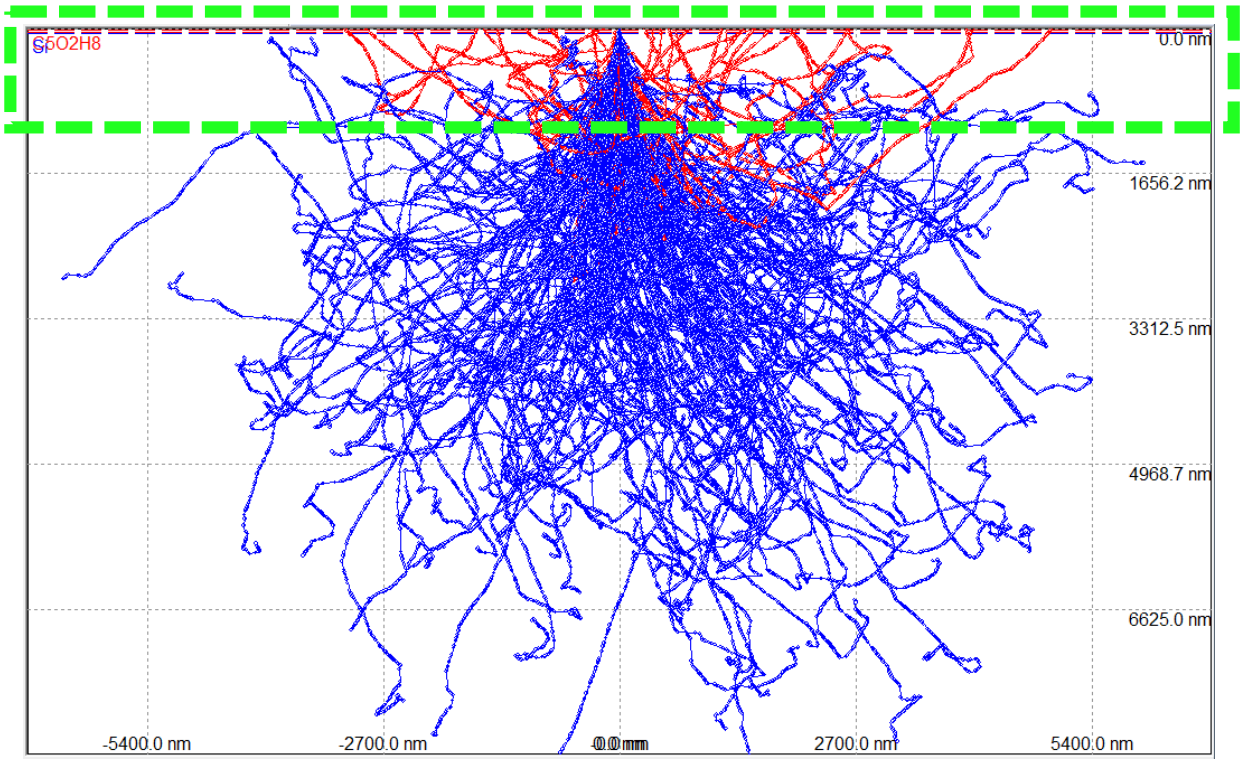

Figure 2.9: Monte Carlo simulation of a 30kV electron beam incident on a silicon wafer with a 30nm film of PMMA. The blue lines represent the primary electrons, the red lines represent the escaped backscattered electrons, and the green box represents the area displayed in figure 2.10.

Therefore, a 30nm film of PMMA, the specific resist used in this thesis work, is located on top of a silicon substrate and a 30kV beam of electrons is incident on the sample.

Figure 2.9 shows the entirety of the generated excitation volume where blue lines represent primary electrons and red lines represent backscattered electrons which escaped the sample. The green box represents the magnified area displayed in figure 2.10. In figure 2.10, the primary beam is shown penetrating through the resist and experiencing minimal forward scattering from the resist. Backscattered electrons generated in the substrate, however, penetrate a large area of the resist as these electrons exit the sample. It is important to note that while secondary electrons are not displayed in this simulation, they can be generated by any displayed primary or backscattered electron path because they only require approximately 5-50eV to be excited. Since the energy required to perform chain scission of a carbon-carbon PMMA bond is less than 5eV [18], PMMA exposure is performed by primary, backscattered, and secondary

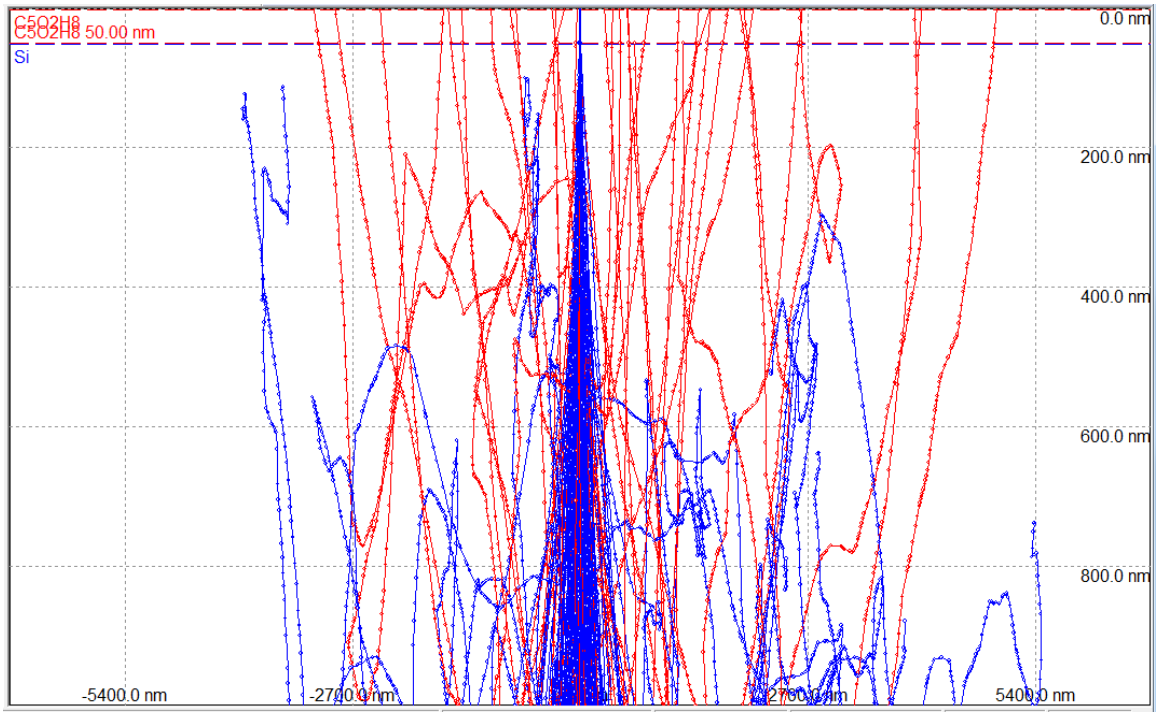

Figure 2.10: The surface micron of the Monte Carlo simulation shown in figure 2.9.

electrons. Therefore, the resolution of electron-beam lithography is not determined by the primary beam spot size, but rather by the scattering of the primary beam inside the resist and the substrate.

2.3 Atomic Force Microscopy

An AFM is a subsection of microscopes under the broader SPM (scanning probe microscope) category. An SPM is a microscope identified by two main qualifiers: a physical probe is scanned over a sample to generate an image and these scan motions are generated through piezoelectric crystals. The information gained from the scan is determined by which

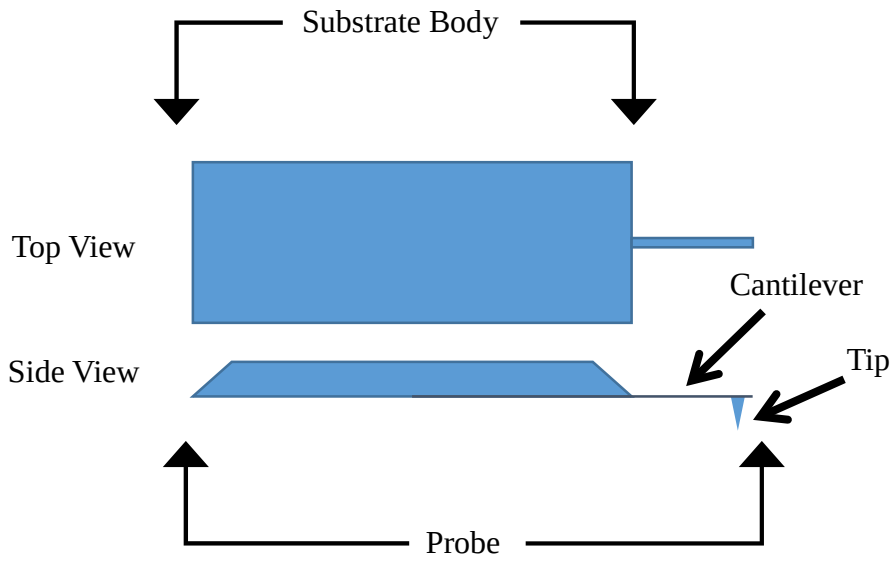

Figure 2.11: Top and side view illustrations of a typical AFM probe.

probe is used and which tip-sample interaction is examined [19]. An AFM generally utilizes a silicon probe of the geometry shown in figure 2.11. The substrate body is typically of dimensions 3.5mm x 1.5mm x 0.3mm, the cantilever of dimensions 120µm x 40µm x 4µm, and the tip of 15nm radius and length of 12µm [20]. This probe is mounted to set of piezoelectric crystals and made to scan over the surface of a sample while oscillating in the z-axis direction.

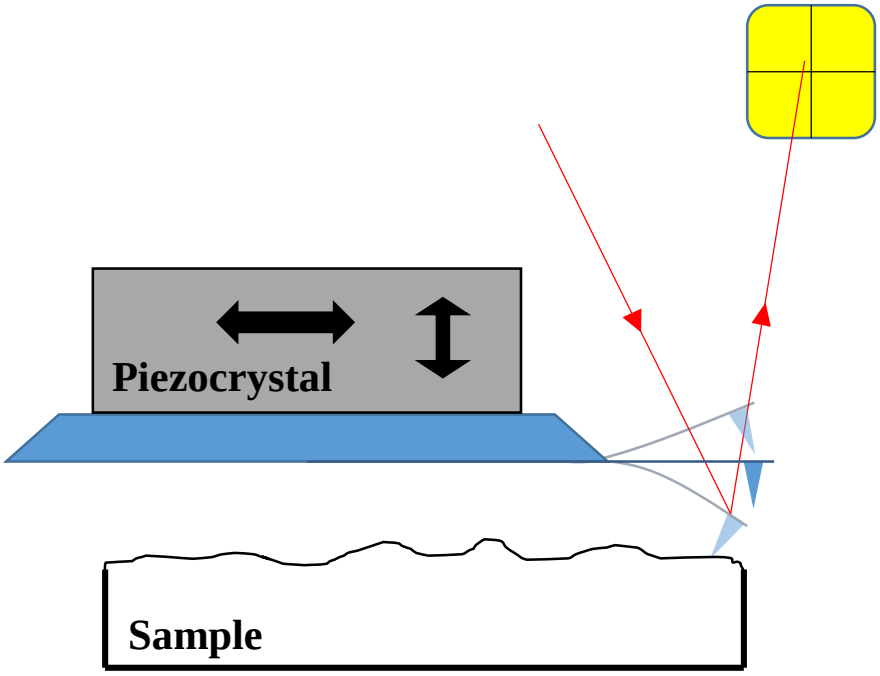

Figure 2.12: AFM cantilever oscillations are monitored by reflecting a laser off of the cantilever and onto a position-sensitive photodiode detector.

The vibrations of the substrate body cause the cantilever to deflect, and these movements are monitored by reflecting a laser off of the top of the cantilever and onto a position-sensitive photodiode detector as shown in figure 2.12. If the cantilever is oscillated in free space then the detector observes a sinusoidal response from the reflected laser. This represents a cantilever deflection of consistent amplitude and frequency, and this frequency corresponds to the harmonic frequency of the cantilever. As the tip is brought near the sample surface, it experiences various attractive and repulsive forces. The attractive van der Waals forces are felt within a few hundred angstroms of the sample surface, and this attractions strengthens exponentially as the tip-sample distance decreases. When the tip is pushed into the sample by the cantilever, the tip experiences strong repulsive forces from the inner electron shells of the tip and sample repelling each other. This repulsive force dominates the attractive forces when the tip contacts the sample. As the tip scans the sample and taps the surface with each oscillation, it

experiences attractive and repulsive forces [21]. These forces modify the tip oscillations and these modifications are detected as a change in amplitude and frequency of the tip movements. The detector is connected to the piezoelectric crystals in a feedback loop and the height of the probe is adjusted so as to maintain a constant cantilever oscillation amplitude. An AFM height image is a compilation of points whose positions are relative to the position of the probe tip on the sample and whose brightness are determined by the relative height of the probe as determined by the z-axis piezoelectric crystal at that respective scan point [22].

This form of AFM imaging is called tapping mode because the probe taps on the sample with each oscillation. It is considered a nondestructive mode of imaging as the tip-sample forces are of a very low magnitude [23].

2.4 Magnetic Force Microscopy

MFM (magnetic force microscopy) is another subsection of SPM imaging and is performed in a similar manner to AFM imaging. The same probe is used as in AFM but the tip is coated with a thin magnetic film, as shown in figure 2.13. A magnetic image is gathered by performing two scans of the same sample area. The first scan is a standard AFM tapping image to determine the topography of the sample. The second scan is called the interleave scan and is performed at user-specified height above the sample surface called the lift scan height, and is illustrated in figure 2.14. As the interleave scan progresses, the height of the probe is

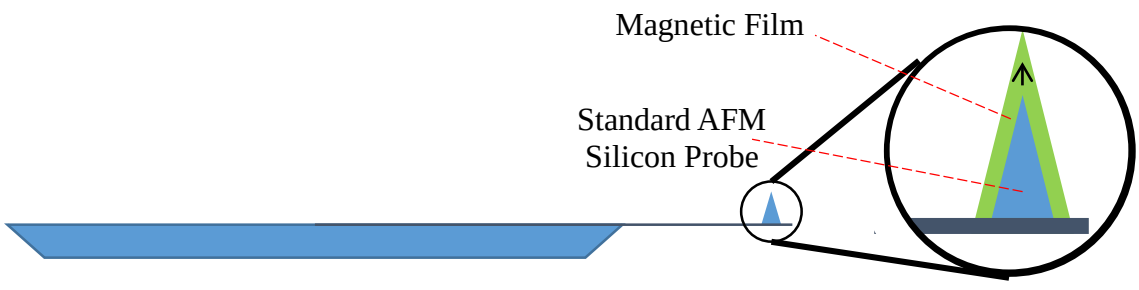

Figure 2.13: A side view of an MFM probe. The tip is coated in a magnetic film.

continuously adjusted so as to maintain a constant tip-sample distance based off the previously-gathered height image and the specified lift scan height. This effectively neutralizes the effect of the van der Waals forces by keeping them constant. Any manipulation of the cantilever amplitude or frequency must then instead be caused by the magnetic interaction between the tip and the sample, and this is illustrated in figure 2.15. These modifications are observed by the detector and a magnetic image is obtained [24]. Table 2.1 identifies and describes important parameters manipulated and maintained during a scan to achieve an optimal image [25].

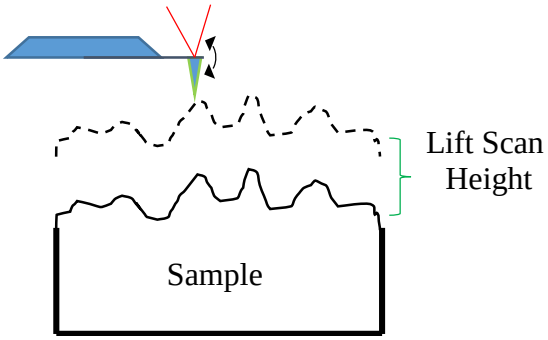

Figure 2.14: The interleave scan follows the topography of sample as determined by the initial tapping mode scan.

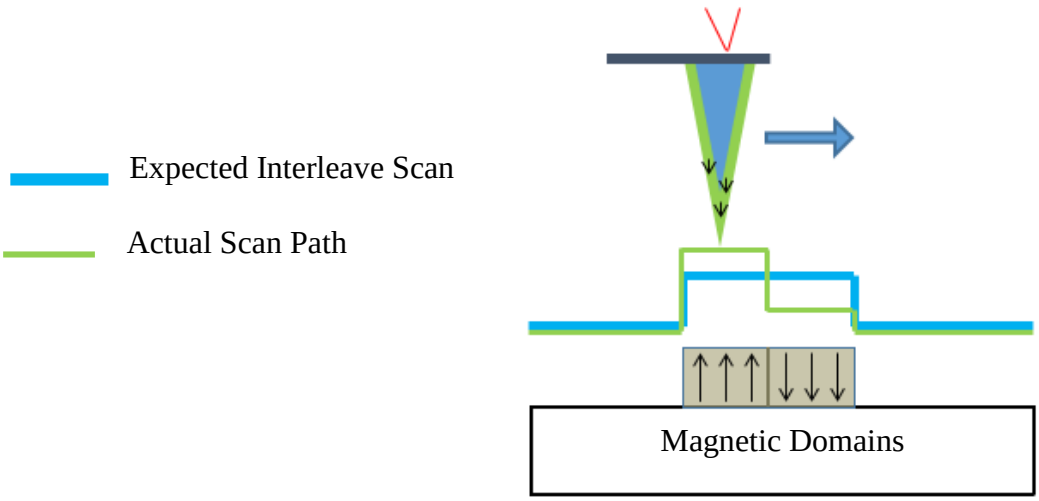

Figure 2.15: The blue line shows the expected interleave scan path as determined by the topographical image. The green line shows the actual interleave scan path as determined by the magnetic nature of the feature.

Table 2.1: Important AFM/MFM scan parameters and their definitions.

Parameter	Setting
Scan Rate	The frequency of each scan line. The scan size of an image, scan rate, and tip velocity can all be controlled through the scan menu but only with two degrees of freedom. The scan rate is given here and the scan size is shown in the image. Therefore, the tip velocity could be calculated if desired.
Drive Frequency	The frequency of the drive signal applied to the z-axis piezoelectric crystal and subsequently the frequency of the cantilever oscillations. This value should equal the harmonic frequency of the cantilever.
Drive Amplitude	The amplitude of the feedback signal supplied to the z-axis piezoelectric crystal to maintain the desired tip oscillation amplitude.
Lift Scan Height	The lift distance of the interleave scan during MFM relative to the sample surface.

Chapter 3: Application of Samples

As mentioned in chapter 1, this section is not meant to be a comprehensive review of the applications of the samples presented in this thesis, but rather a brief primer so that the fabrication and characterization process can be better understood within context. Therefore, a brief introduction and explanation will be given for each of the three samples and the chapter will be concluded.

3.1 Domain Wall Memory

DWM (domain wall memory) is a reincarnation of bubble memory systems from the 1970s. The original bubble memory was a magnetic memory device where a bit of data was carried by a magnetic domain. Parallel lines of magnetic material were spanned across a substrate, and one end of the substrate contained a read assembly and the other end a write assembly. An external magnetic field propagated the domains along the lines. While data was still read in a serial fashion, it was done so at a fast rate because the large rotating disc used with HDDs was eliminated [26]. The introduction of semiconductor-based memory devices, the improved data capacity of HDDs, and the durability of emerging flash RAM technology, however, brought bubble memory to irrelevancy.

In DWM devices, the same magnetic lines are used to store and transmit data but at a smaller scale because of technological improvements in the magnetic read/write field. Data is stored in domains, and the length of the domain corresponds to the bit length. Pinning sites are designed into the wire to control this bit length by allowing domains to form at the pinning sites.

A polarized current is input to the wire to move these domains and the domains move predictably because of these pinning sites. Domain walls could theoretically be constructed in a three-dimensional layout to maximize bit density. Considering the large storage density, the high-speed access of information, and the non-volatile, durable nature of magnetic storage, researchers are investigating the use of DWM as a potential universal memory device [27, 28].

The fabrication and characterization of the DWM device in this thesis was performed as a proof-of-ability task for a potential collaboration with a research group from another university. Therefore, this sample was complete when a nanowire was formed and domains were observed at the notches designed into the wire.

3.2 Physically Unclonable Function

A PUF, or physically unclonable function, is defined in [29] as "an expression of an inherent and unclonable instance-specific feature of a physical object." Therefore, the essence of a PUF is that its intrinsic uniqueness is inherently created upon fabrication of the PUF. These devices are meant for use in security and authorization systems because they provide an output, or response, that is unique and unpredictable to a given input, or challenge. As a matter of feasibility, a PUF should be simple to fabricate and evaluate, but nearly impossible to reproduce [30]. In this manner, a PUF can be considered as an "object's fingerprint" [29].

A simple example of a PUF device is the optical PUF using air-impregnated epoxy. To make this device, a puck of epoxy is injected with air while hardening to produce a bubble-riddled transparent puck. When light is transmitted through the epoxy puck, a unique pattern will project onto a display screen. As the angle of the incident light is changed, the display pattern changes as well. The projected pattern can be characterized as a function of the incidence angle and a PUF created. A given angle of incident light (challenge) will reliably

produce a specific display pattern (response), but this response will not be easily guessed or replicated by a foreign source.

The PUFs created in this thesis are magnetic PUFs. This device is founded on the basis that inherent defects in the lithography process will give individual single-domain magnetic cells shape asymmetry, and this asymmetry will result in a preferred ground state for a given cell. Since the defects are random, the shape asymmetry varies from cell to cell. Therefore, the preferred state of a given cell should be random but consistent. Random cells can be picked from the array as the challenge, and their respective collective Boolean ground states will be known but not easily predicted by a foreign source.

The PUF sample was meant to be an array of decoupled nanomagnets which displayed random but consistent magnetic behavior. To realize this, the array needed to be clocked in a purely hard-axis direction. The easy axis of a magnet corresponds to the state of lowest energy of the magnet and lies in the direction of the aligned moments in the absence of an applied field. The hard axis, therefore, is the direction of moments when the magnet is in its highest state of energy and is typically in a direction perpendicular to the easy axis. In context of this work, clocking describes the process of applying a magnetic field to a nanomagnet in the direction of the hard axis of the nanomagnet. This is done with the intention of forcing the nanomagnet to an unstable state so that it can settle to the state of lowest energy.

Since each cell within the array is decoupled from its nearest neighbor, the array contains a group of individual, isolated nanomagnets. Therefore, after each the array is clocked, it will settle to a state where each nanomagnet is in its lowest-energy ground state as a product of the applied clocking field and the shape asymmetry of the nanomagnet. The objective of the characterization of the PUF samples in this thesis, however, was simply to observe randomness

within the array after clocking events. Consistent randomness was not experimentally critical yet, and is rather the first goal of the future work to be performed on the PUF samples. SEM and MFM images of the arrays were sent to other members of the research group for analysis and simulation studies.

3.3 Vision

The Vision patterns represent a novel approach to image recognition. Image recognition by a computer is generally performed in the following manner: receive an image, identify lines and segments in the image, group related segments together, and use grouped segments to match features to database of known images. For a computer, the most computationally-difficult and time-consuming step in this process is the grouping of related segments. The Vision sample aims to solve this lengthy quadratic optimization problem by observing the magnetic state of an array of intentionally-placed nanomagnets. The states of each magnet will determine if features and edges in an image are related or unrelated, and the grouped-edge image can then be externally processed and identified [4, 5, 31, 32].

This project is still in an experimental phase and specific arrays were patterned for specific images to be identified. Each cell within the array would be a magnetic nanodisc of precise diameter. This would allow the cell to settle in a vortex state when sufficiently isolated, but in a single-domain state when sufficiently coupled with neighboring cells. In this manner, related cells can be determined from the final magnetic state of the system. This diameter was chosen as a result of the studies performed by Cowburn *et al.* in [33].

The objective of the characterization of the Vision sample in this thesis was to continue the verification and optimization of the Vision problem. The MFM images of the individual arrays were sent another member of the research group for analysis and interpretation.

Chapter 4: Fabrication

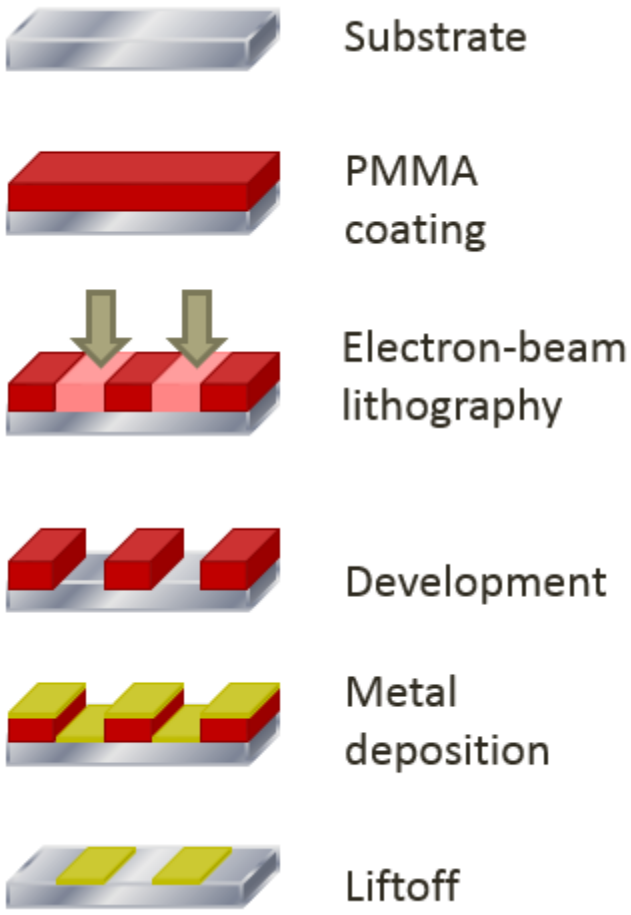

Figure 4.1: The fabrication process flow.

4.1 Design Pattern

Creating a pattern for EBL is listed as the initial step but it is not imperative that this be completed first. The other steps need to be completed in the order listed, but this step can be performed at any time prior to exposure. Therefore, it is listed first simply to avoid arbitrarily disrupting the process flow at a later step.

All patterns were created using an NPGS-packaged version of DesignCAD. This version allows the CAD files to be saved with a ".NPGS" extension which can then be imported into the NPGS software. This enables the NPGS software to control the SEM scan coils to transfer the designated pattern to the photoresist during lithography. The lithography was performed at a standard magnification of 1,000x, thus implying a 100μm x100μm raster area. Patterns were therefore designed to accommodate a write area of this size. Features can be assigned a color in the CAD software and this color will be used to define the dosing parameters during exposure. A single color does not explicitly dictate a specific dosing value, but rather dosing values are specified on a per-exposure basis. A star with two arrows was included in each pattern file so that the pattern area could be more-easily located during device characterization.

For the sake of continuity and clarity, the following terms will propagate throughout the remainder of this thesis when discussing the fabricated samples: cells or elements are the building block of the fabricated samples and are the individual nanostructure entities; arrays designate a group of cells or elements arranged in a periodic fashion; and patterns designate the entire file created in DesignCAD and includes all cells, arrays, landmarks, and extra features. Three families of patterns were created (DWM, PUF, and Vision) amongst four different samples.

4.1.1 DWM

The essence of the DWM pattern was a 15μm long magnetic nanowire with tapered ends and 11 notches periodically designed into a single side. The width of the wire was 200nm. The notches had a 150nm wide base, a 60nm protrusion depth into the nanowire, and a 1.15μm spacing. These dimensions were chosen according to the dimensions shown in [27]. Since a single nanowire is considerably smaller than the write area, multiple wires were integrated into

(a)

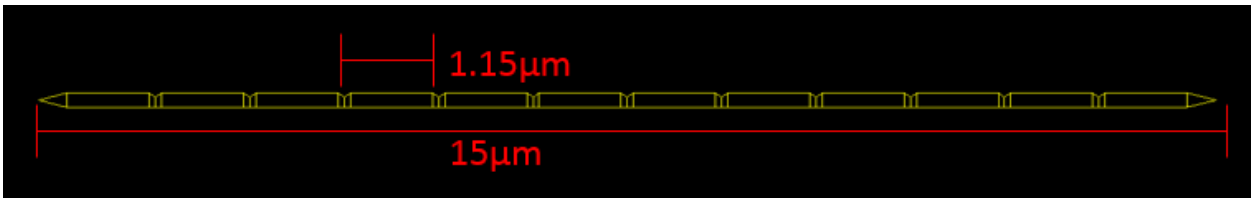

(b)

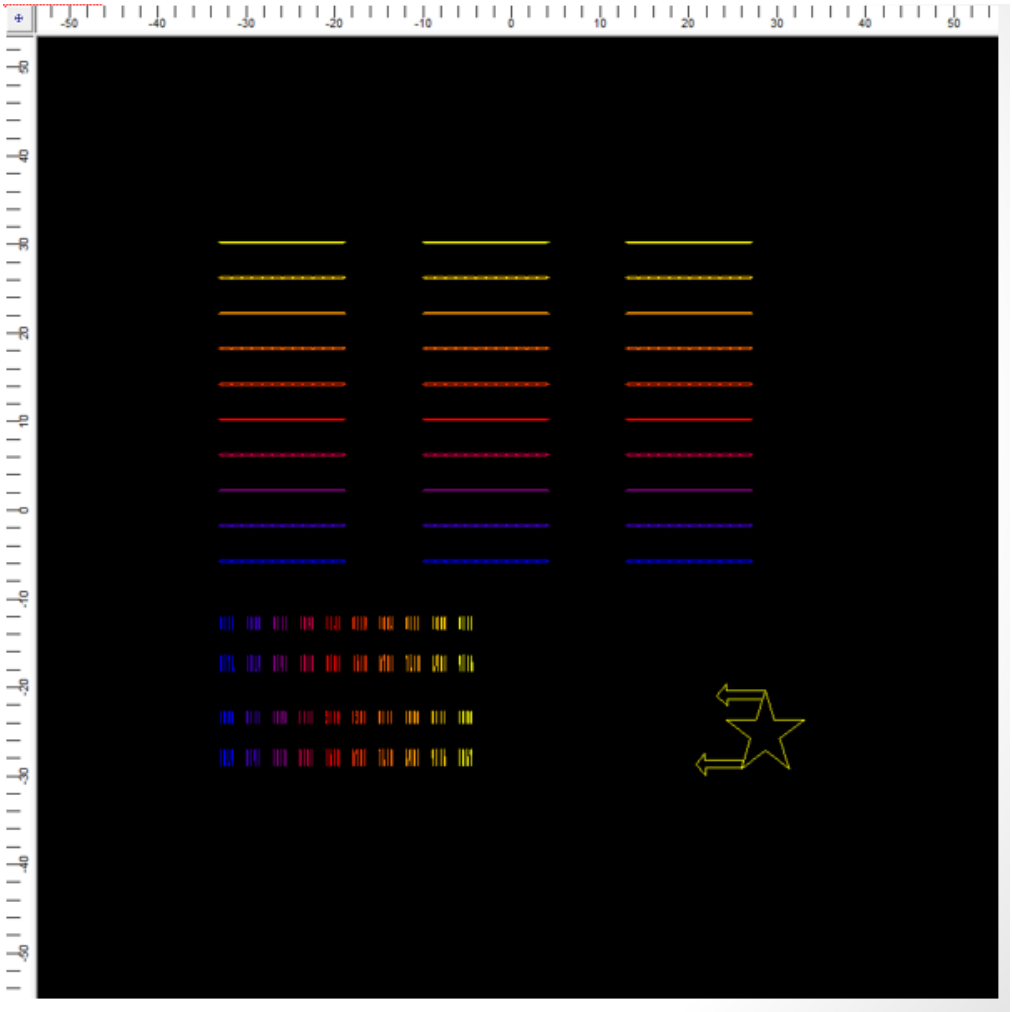

(c)

Figure 4.2: DWM CAD pattern. (a) Shows part of a single nanowire, (b) shows an entire nanowire, and (c) shows the entire pattern.

a single pattern. A total of 30 wires were used per pattern and arranged in a 3x10 array. The color of each row was adjusted and each column was identical. This was done for the sake of repetition within each pattern. The small array located below the nanowire array was not used in this thesis and can be ignored.

4.1.2 PUF

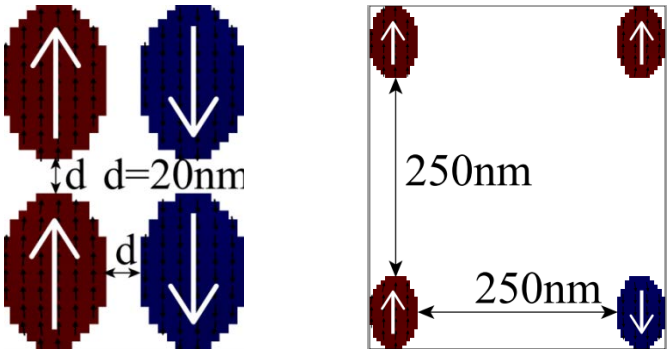

Figure 4.3: Simulation showing the necessary feature spacing to achieve decoupled magnetic behavior. OOMMF simulation performed by Jayita Das.

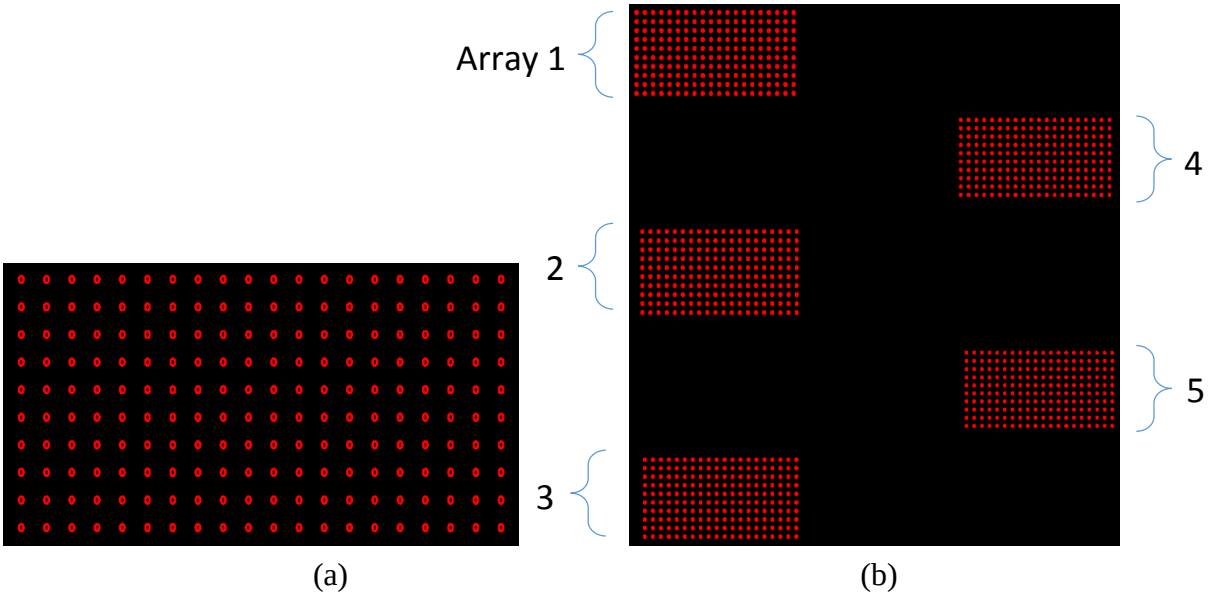

Figure 4.4: (a) Shows a single PUF-1 array. (b) Shows and labels all five PUF-1 arrays.

Table 4.1: Cell dimensions and cell spacings of each PUF-1 array.

Array	Cell Dimensions	Cell Spacing
1	100 x 67 nm^2	300nm
2	90 x 60 nm^2	300nm
3	80 x 53 nm^2	300nm
4	70 x 47 nm^2	300nm
5	60 x 40 nm^2	300nm

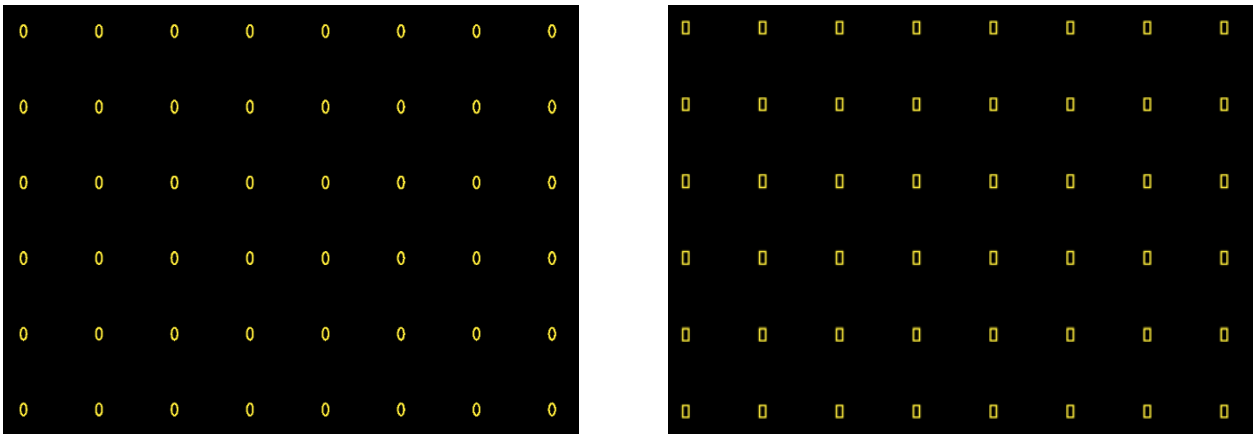

Figure 4.5: (a) and (b) show the PUF-2 elliptical and rectangular arrays, respectively.

Table 4.2: Cell dimensions and cell spacings of each PUF-2 array.

Array	Cell Shape	Cell Dimensions	Cell Spacing
1	Ellipse	100 x 50 nm^2	300nm
2	Rectangle	100 x 50 nm^2	300nm
3	Ellipse	80 x 40 nm^2	300nm
4	Rectangle	80 x 40 nm^2	300nm

A sample fabricated according to a PUF pattern should produce an array of decoupled magnetic nanostructures. The simulation from figure 4.3 was performed by another member, Jayita Das, of the research group using OOMMF and shows that the intra-array spacing of these structures needed to be at least 250μm to achieve a decoupling behavior and the patterns were designed accordingly. The PUF-1 pattern is shown and described in figure 4.4 and in table 4.1. The PUF-2 pattern is shown and described in figure 4.5 and in table 4.2.

4.1.3 Vision

The essence of the Vision pattern was five distinct arrays of tightly-spaced magnetic nanostructures with circular geometries. Each array began as 1024 cells originally placed in a 32x32 fashion with each cell having a diameter of 145nm and nearest-neighbor spacing of 20nm. This array was replicated four times. Individual cells were then deleted from each array so that a unique and specific pre-designated layout could be achieved. The final arrays contained 200-300

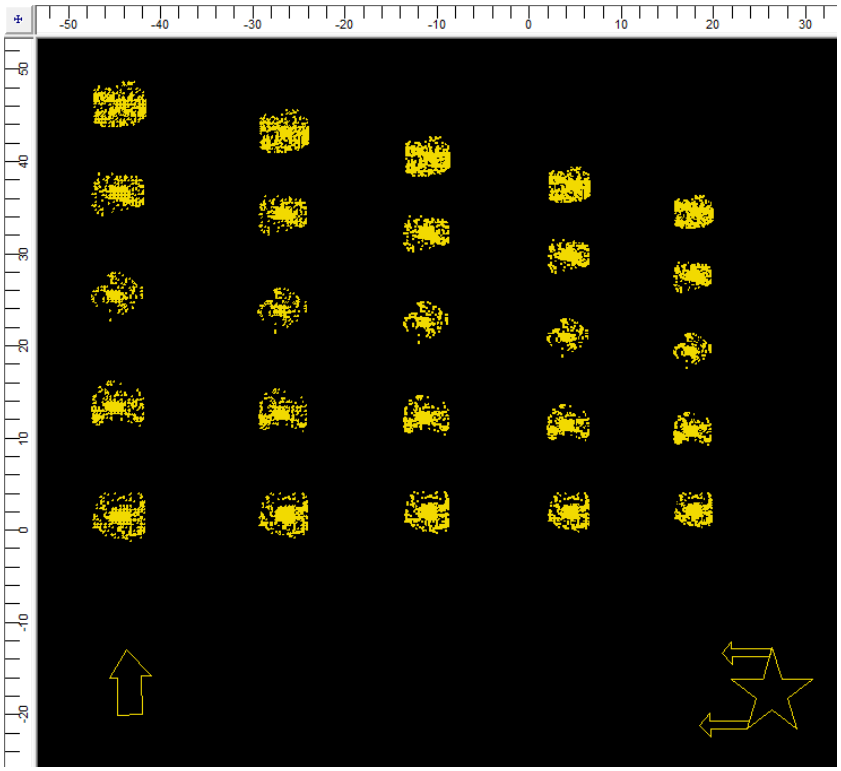

Figure 4.6: The entire Vision pattern.

cells and each array was then scaled d own in size so that each cell had a diameter of 135, 125, 115, and 105nm but maintained a 20nm spacing. A vision pattern therefore contained 25 arrays total. As usual, the star feature was added to the bottom right of the pattern for use as a landmark for post-fabrication pattern location. The vision pattern is shown in figure 4.6.

4.2 Photoresist

All samples were fabricated on n-type <100> silicon wafers. PMMA, or poly(methyl methacrylate), is the standard electron beam lithography resist [34] because of its ease of use and its high resolution results and MicroChem 950PMMA A7 was therefore used as the resist for all samples. Higher molecular weight PMMA allows for higher resolution lithography, and the 950kDa resist purchased was the highest commercially-available resist from MicroChem. The A7 designator signifies that the solution is 7% PMMA solids in anisole and this corresponds to an ultimate film thickness of 300nm when spincoated at 5,000rpm [35]. The rule of thumb for spinning PMMA as an EBL resist is to target a resist thickness of three times thicker than the desired feature thickness. Since the DWM sample was to be 40nm thick and the PUF and Vision samples were to be 10nm thick, PMMA films of 120nm and 30nm were desired. The A7 solution was diluted with pure anisole according to the spin-speed curve shown in [35] so that the desired resist thickness would be achieved.

Throughout the track of the work performed in this thesis two separate resist spin coaters were used (Laurel Technologies WS-400-6NPPB and Integrated Technologies P-6204). The Laurel spinner was located in a fume hood inside a class 1000 cleanroom and fitted with a 2" wafer chuck for spinning 2" wafers. The P-6204 spinner was located in a fume hood in a non-cleanroom environment and fitted with a 3mm chuck for spinning small wafer squares. Table 4.3 shows the spinning procedure and tables 4.4 and 4.5 show specific recipes for the Laurel spinner and the P-6204 spinner, respectively.

Table 4.3: Photoresist spin procedure.

Step	Duration
Solvent clean wafers using acetone, isopropyl alcohol, and methanol alcohol and rinse with DI water	10 seconds each
Dry with nitrogen gas	10 seconds
Bake on hotplate at 110°F	60 seconds
Mount onto spin coater chuck	----
Follow spin recipe	Refer to tables 4.2 and 4.3
Measure thickness	----
Bake on hotplate at 110°F	60 seconds

Table 4.4: Laurel spinner recipe.

Step	Duration
Ramp up to 500rpm	5 seconds
Ramp up to 6,000rpm	10 seconds
Spin at 6,000rpm	45 seconds
Ramp down to 0rpm	15 seconds

Table 4.5: P-6204 spinner recipe.

Step	Duration
Ramp up to 5,000rpm	10 seconds
Spin at 5,000rpm	60 seconds
Ramp down to 0rpm	20 seconds

4.3 Exposure

A 1cm^2 piece of wafer was mounted to a 1" aluminum SEM holder using two copper clips. A 3mm hole had been drilled into the face of the holder, filled with carbon glue and covered with a TEM grid. This would act as a Faraday cup to accurately measure the primary beam current (an important parameter for lithography). A diamond scribe was used to make a small scratch on an edge of the wafer to be used as a landmark designator during exposure and characterization. The sample was inspected with an optical microscope to verify the quality of the resist film in the designated pattern-write area.

The Hitachi SU-70 SEM was retrofitted with Nabity NPGS (Nanometer Pattern Generation System) by JC Nabity Lithography Systems. The CAD patterns designed for each sample were imported to the NPGS system and internally converted to a run file which could be used to position the primary beam according to the pattern. The sample was loaded into the SEM chamber and the beam was aligned, stigmated, and focused on the Faraday cup. The beam current was measured and then the beam was moved to the pattern writing area.

Contamination spots were grown by inputting a null signal to the scan coils. This forces the beam to dwell at one point and the beam will deposit contamination from the sample and chamber onto this point. The geometry of this spot will reflect the geometry of the beam and the beam can be fully-optimized by using these contamination spots as a reference [36]. When optimized, the stage was moved 200μm and a pattern was drawn. The stage was then moved another 200 μm and another contamination spot was grown to rectify defocusing caused by a slight height gradient across the sample surface. This process was repeated until all patterns for a sample had been written. The beam and exposure parameters used during lithography for each sample are shown in tables 4.6-4.9.

Table 4.6: Exposure parameters for DWM sample.

Parameter	Value
Accelerating Voltage	30kV
Emission Current	47µA
Landing Current	28.3pA
Working Distance	6.4mm
Magnification	1,000x
CCD	5nm
LS	5nm
Dose	100-1,800µC/cm2
Dwell time	0.7405-4.4427µs

Table 4.7: Exposure parameters for PUF-1 sample.

Parameter	Value
Accelerating Voltage	30kV
Emission Current	41µA
Landing Current	29.4pA
Working Distance	6.4mm
Magnification	1,000x
CCD	5-10nm
LS	5-10nm
Dose	300-1,200µC/cm2
Dwell time	2.1382-46.5661µs

Table 4.8: Exposure parameters for PUF-2 sample.

Parameter	Value
Accelerating Voltage	30kV
Emission Current	50µA
Landing Current	23.7pA
Working Distance	6.4mm
Magnification	1,000x
CCD	5nm
LS	5nm
Dose	250-350µC/cm^2
Dwell Time	2.2104-3.0946µs

Table 4.9: Exposure parameters for Vision sample.

Parameter	Value
Accelerating Voltage	30kV
Emission Current	50µA
Landing Current	23.7
Working Distance	6.4mm
Magnification	1,000x
CCD	5nm
LS	5nm
Dose	250-350µC/cm2
Dwell Time	1.2988-4.2724µs

4.4 Photoresist Development

The sample was developed using MIBK (methyl isobutyl ketone). This solvent penetrates into the resist and forms a gel. A polymer chain is removed from the polymer matrix when engulfed by this solvent [37]. Longer chains are more affixed to the matrix and will therefore take more time to remove [38]. A strong developer is able to remove the longer chains of resist and this blurs the contrast between exposed and unexposed resist areas. Diluting the MIBK with IPA has been shown to increase the selectivity of the resist by decreasing the ability of the developer to dislodge large chains of resist from the matrix. Literature shows that a 3:1 IPA:MIBK mixture produces optimal developer contrast [39] and 10mL of this solution was used to develop each sample for 30 seconds.

4.5 Thin Film Deposition

An electron beam evaporator was used to deposit a thin film of permalloy onto the sample. Permalloy ia an 80%Ni-20%Fe alloy and was chosen for use in this thesis because of its high permeability and low coercivity ferromagnetic behavior [40]. Figure 4.9 shows a cross-sectional view of a typical electron beam evaporation system. The sample was installed facedown onto the sample holder and loaded into the chamber at a distance of 30cm above the permalloy source. The chamber was pumped down to a pressure of 1μTorr. This pressure corresponds to a mean free path length of a few meters and will minimize the scattering of particles to a negligible amount.

A beam of electrons was generated through thermionic emission from a tungsten filament and positioned onto the source using permanent magnets and electromagnets. This beam transferred energy to the source and caused the source to increase in temperature, resulting in the melting and evaporation of the source. Due to the large mean free path length within the

chamber, the gaseous source material condensed on everything within a line-of-sight view of the source. This deposition rate was monitored with a quartz crystal microbalance and evaporation was stopped when the desired thickness of 10nm (PUF and Vision) or 40nm (DWM) had been achieved. The electron beam was maintained at a bias 7.5kV and emission current of 40mA, producing a deposition rate of 0.3Å/sec.

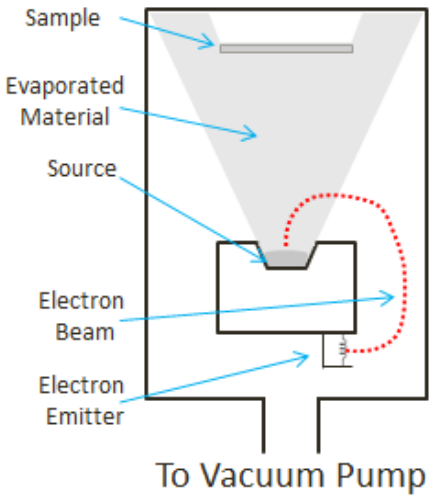

Figure 4.7: Cross-sectional view of an electron beam evaporator.

4.6 Liftoff

The liftoff process was completed to remove all materials that were not included in the post-fabrication design. This entails photoresist and the permalloy deposited onto the unexposed photoresist. Acetone dissolves the resist and thereby removes the permalloy on top of the resist from the sample. The acetone will not react with or interfere with the permalloy deposited directly onto the substrate. The sample was placed in a beaker filled with 50mL of acetone and the beaker was placed in an ultrasonic bath. The agitation promoted proper dissolution of the resist and subsequent liftoff of the metal. The sample was removed from the beaker after 10 minutes, rinsed with IPA and dried with nitrogen gas.

Chapter 5: Characterization

The characterization of samples was performed using an SEM and MFM. The objective of the SEM characterization was to identify and capture topographical images of high-quality patterns. The objective of the MFM characterization was to obtain a magnetic image of these high-quality patterns. The SEM used during characterization was the Hitachi SU-70 Schottky-type emitter SEM, and the MFM used during characterization was the Digital Instruments 3100 AFM in MFM mode.

A high-quality pattern would consist of nanostructures of identical geometries, dimensions, and orientations as the respective CAD file, and these nanostructures would be affixed to a clean, defect-free substrate. Naturally, any deviation from this circumstance would constitute a pattern as low quality. Pattern quality was generally determined qualitatively and then verified quantitatively. Patterns which demonstrated obvious defects were readily identified

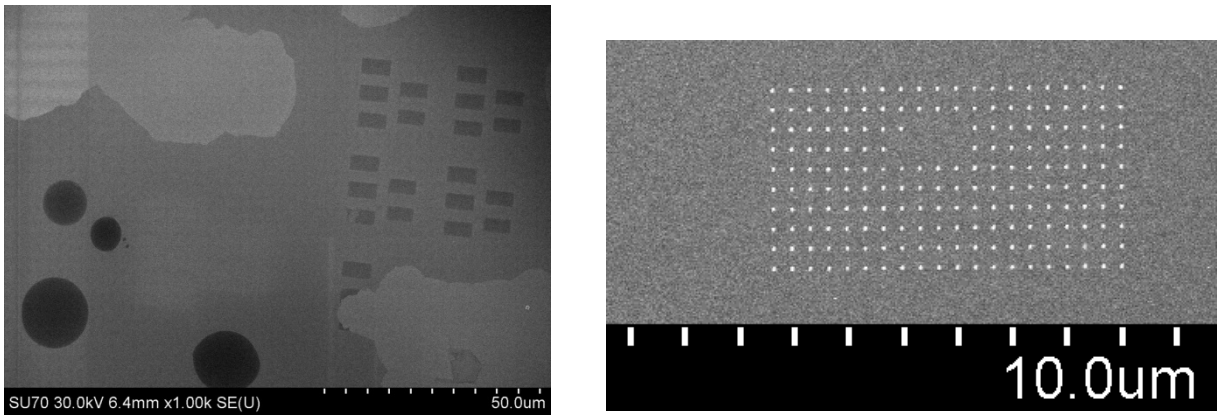

(a) (b)

Figure 5.1: (a) Shows a sample with liftoff errors, as demonstrated by the splotchy topography. (b) Shows an array with a group of cells missing.

and promptly ignored. Some examples are shown in figures 5.1. The remaining patterns were then examined in a more careful manner and individual geometries were examined. Patterns which displayed geometries and layouts as expected according to the CAD files were measured against their CAD files as confirmation of their quality. Patterns with similar dimensions to the CAD files deemed high quality and patterns with dissimilar dimensions were deemed low quality. Images were captured of these high-quality patterns and their locations were noted for future reference.

5.1 DWM

The overall objective of the DWM sample characterization was to obtain a magnetic image of a nanowire that displayed domain formation at the wire notch. The SEM characterization was therefore an intermediate step in the overall goal and was simply used to identify nanowires which displayed proper dimensions according to the CAD file. The primary beam and column parameters used during characterization are shown in table 5.1. Low-quality nanowires are shown in figure 5.2, a high-quality nanowire is shown in figure 5.3 and the lithography exposure parameters used to fabricate the high-quality nanowire are shown in table 5.2.

Table 5.1: Primary beam and column parameters during SEM characterization of DWM.

Parameter	Setting
Accelerating Voltage	30kV
Working Distance	~16mm
Landing Current	~275pA
Objective Lens	Upper (Field-Free)

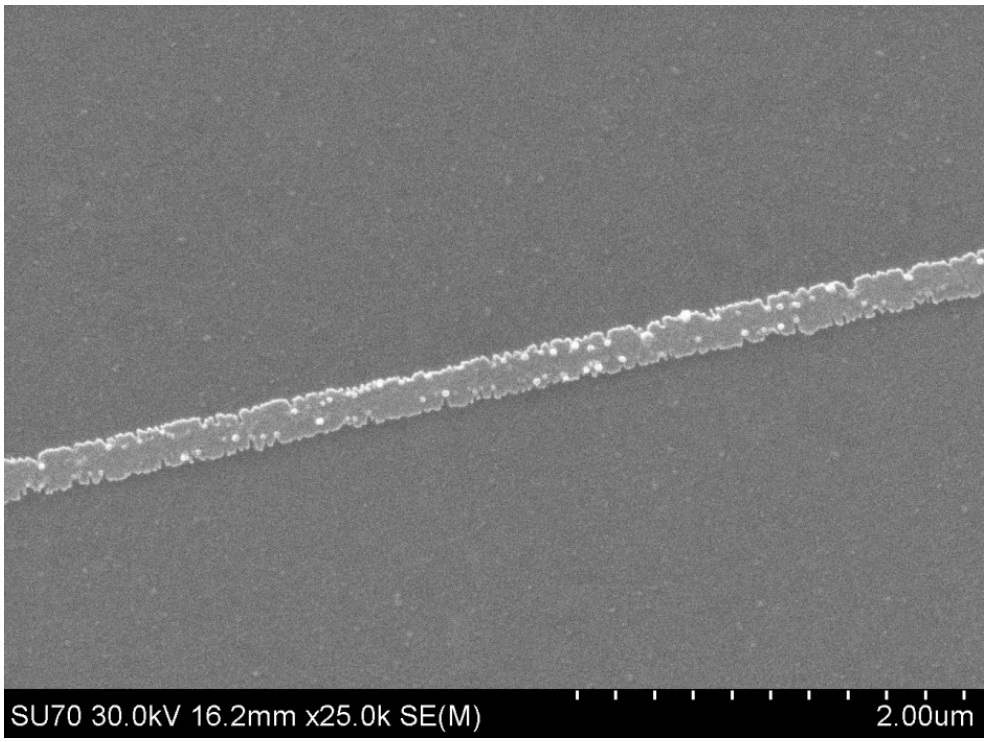

(a)

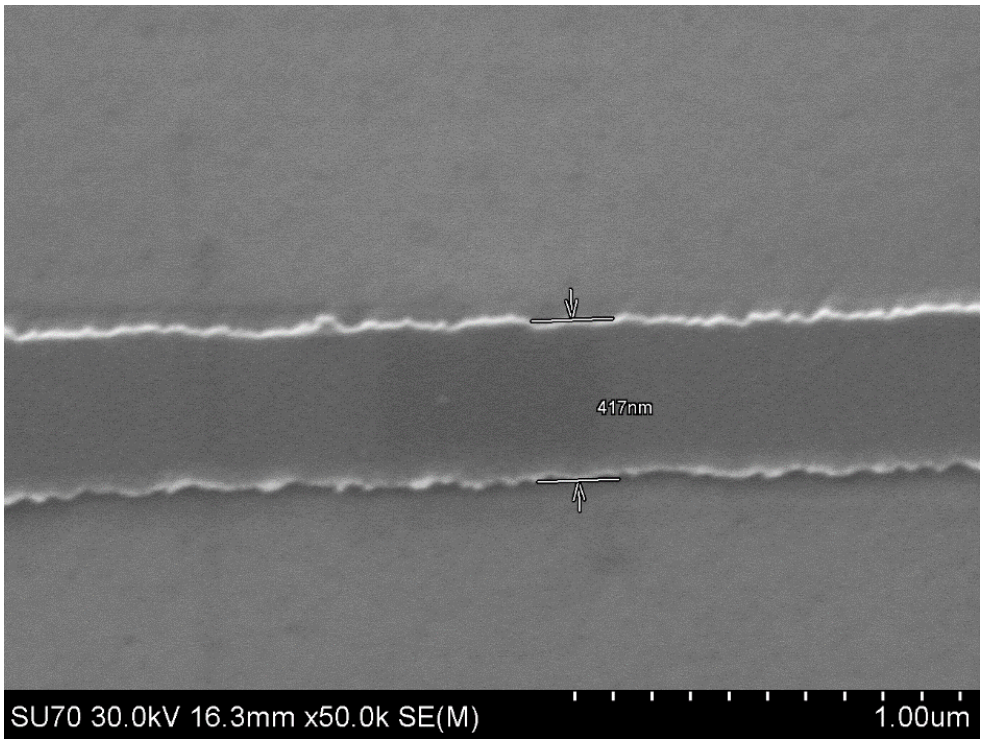

(b)

Figure 5.2: (a) Shows an under-dosed nanowire. (b) Shows an overdosed nanowire.

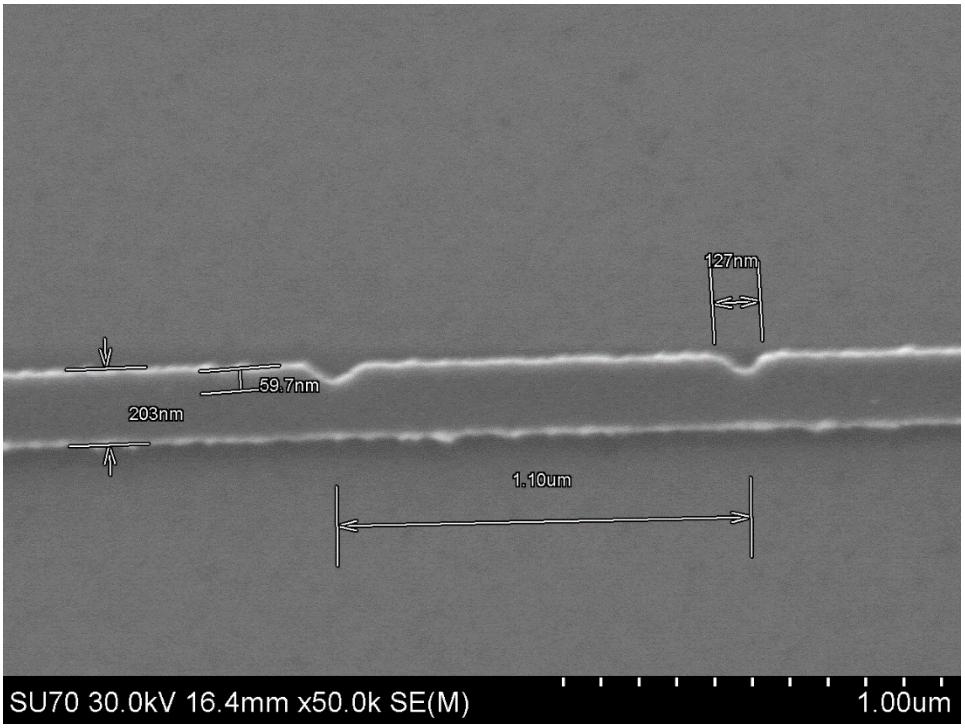

Figure 5.3: A high-quality nanowire shown with proper dimensions.

Table 5.2: Exposure parameters used for high-quality DWM pattern.

Parameter	Setting
Exposure Dose	200μC/cm^2
Dwell Time	1.4809μs
Center-to-Center Distance	5nm
Line Spacing	5nm

The DWM sample was then loaded into the AFM and the standard MESP probe was used to obtain a magnetic image in parallel with a height image of the high-quality nanowires. Figure 5.4 shows two different magnifications of the nanowire and table 5.3 shows the MFM scan

parameters used to obtain the images. Table 2.1 can be referred to for explanations regarding the MFM scan parameters. In each MFM image, it can clearly be seen that domains have formed periodically along the wire in accordance with the notches. Figure 5.5 shows a height image of the nanowire and confirms that the structure thickness is approximately 40nm, as desired. Since this sample was fabricated and characterized simply to demonstrate our ability to do so, the observation of domain-formation at the wire notches concluded the characterization work on this sample.

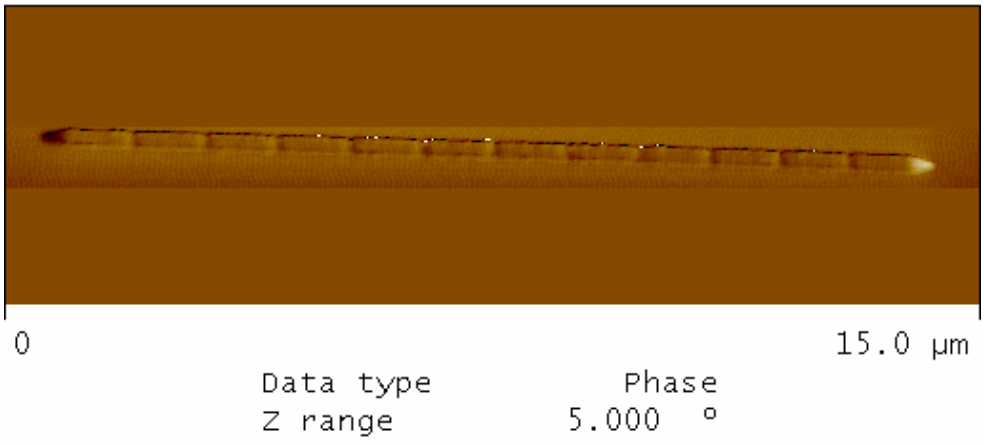

(a)

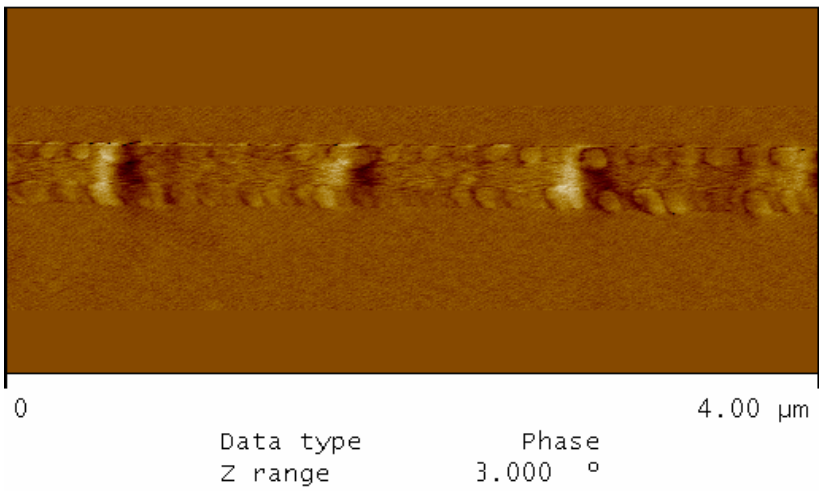

(b)

Figure 5.4: (a) An MFM image of an entire nanowire. (b) Shows an MFM image of a portion of a nanowire.

Table 5.3: Scan parameters used to obtain MFM images of DWM sample shown in figure 5.4.

Parameter	Setting
Scan Rate	0.5Hz
Drive Frequency	61-64kHz
Drive Amplitude	3,500-4,000mV
Lift Scan Height	60nm

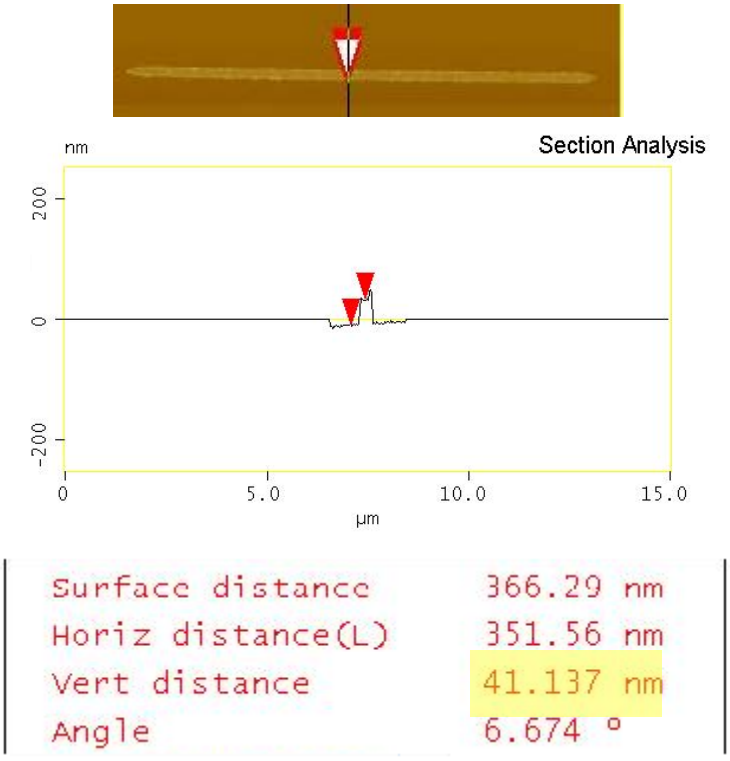

Figure 5.5: A height image of the DWM sample.

5.2 PUF

The two PUF samples were both designed according to the same constraints and guidelines and ultimately provided progress towards the same end-device, but within the scope of this paper they were both characterized according to different objectives. Therefore, the objective of each sample is declared within its respective subsection.

5.2.1 PUF-1

The objective of the SEM characterization of the PUF-1 sample was to identify the fabricated arrays that maintained sufficient intra-array spacings to promote decoupled cell behavior within an array. The objective of the MFM characterization of the PUF-1 sample was to obtain magnetic images of a decoupled array which showed randomness amongst the individual cell states.

Proper dosing was not critical with the PUF samples. Since the PUF-1 features were ellipses, an overdose would simply produce larger-than-expected ellipses. Larger features would produce small inter-feature spacings which could interfere with the decoupling distances designed into the array, but extra inter-feature spacing was given to accommodate for this situation. Therefore, a slight overdose would not interfere with the characterization of the PUF-1 pattern as long as the minimum decoupling distance was maintained.

SEM characterization was performed to identify arrays with proper inter-feature spacing and to capture images of these arrays. These images were used for proper documentation and also sent to other members of the lab for simulation-based studies of the arrays. The primary beam and column parameters used during characterization are shown in table 5.4, arrays with satisfactory inter-feature spacings are shown in figure 5.6, and the lithography exposure parameters used to fabricate the satisfactory arrays are shown in table 5.5.

Table 5.4: Primary beam and column parameters during SEM characterization of PUF-1.

Parameter	Setting
Accelerating Voltage	30kV
Working Distance	~8mm
Landing Current	~250pA
Objective Lens	Lower (Normal)

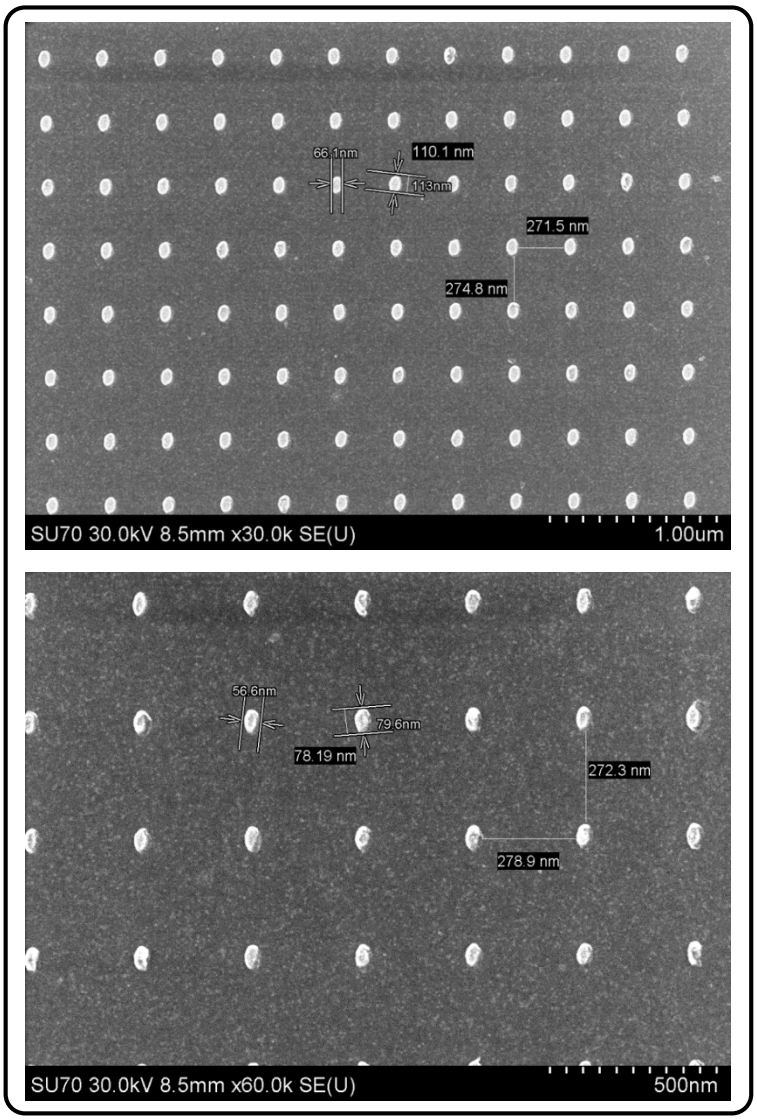

Figure 5.6: PUF-1 arrays with satisfactory inter-feature spacings.

Table 5.5: Exposure parameters used for satisfactory PUF-1 patterns.

Parameter	Setting
Exposure Dose	500-600qμC/cm^2
Dwell Time	3.5637-4.2765 μs
Center-to-Center Distance	5nm
Line Spacing	5nm

A clocking diagram which was of critical importance for the PUF-1 sample is shown in figure 5.7. Case 1 shows two coupled magnetic cells aligned in a parallel state. An external magnetic field (clocking field) is applied to the pair in the in-plane hard-axis direction and the magnetic moment of each cell assumes this same direction. As the clocking field is released, the two cells align in the low-energy antiparallel state due to their coupling energies. Case 2 shows this same original pair of coupled cells but the clocking field has a slight angle bias associated with it (an imperfect clocking field). The individual cells will assume this same bias, but upon

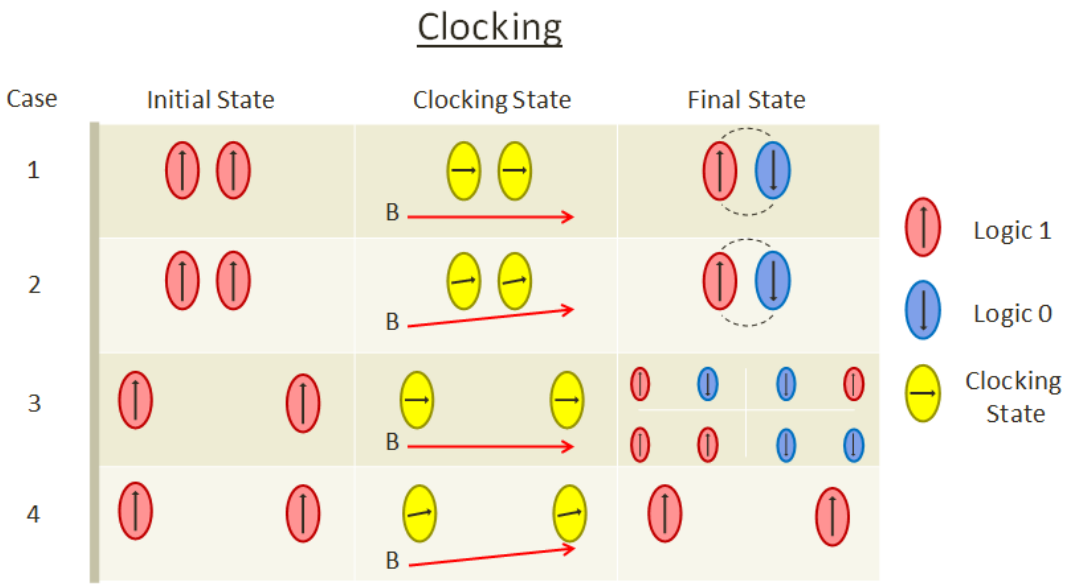

Figure 5.7: Initial versus final states of two magnetic cells subject to clocking field.

removal of the clocking field the cells will still align in an antiparallel state due to their coupling energies. Case 3 shows two decoupled cells with an ideal clocking field applied. Upon removal of the field, either cell can settle randomly to a logic 0 or logic 1 state and four possible combinations can form. Case 4 shows this same pair of decoupled cells but the clocking field has a slight angle bias associated with it. The cells will assume this same bias, and if large enough then the cells will intuitively settle along the direction of this bias upon removal of the clocking field. Therefore, care had to be taken to eliminate this bias during clocking.

The first clocking technique utilized a permanent magnet. The magnet was placed on a plastic stage and a gaussmeter was used to measure the strength of the magnetic field as a function of radial distance from the magnet. The distance corresponding to 45mT was marked. The sample was orientated on a similar plastic stage so that the hard axis of the array was parallel to the magnetic field lines from the magnet and brought to the 45mT designator for 10 seconds, then slid away from the magnet. The setup is shown in figure 5.8.

The sample was then imaged in the MFM using the standard MESP probe and the image in figure 5.9 was achieved. There appeared to be multiple domains in each cell, but this was a result of the tip switching the state of the magnets with every scanline. The magnetic strength of the tip was too great and therefore needed to be reduced to obtain an accurate image. Therefore, the sample underwent the same clocking technique shown in figure 5.8 and was then imaged in

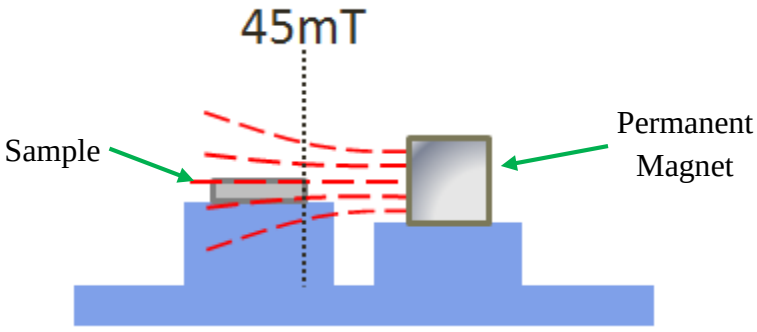

Figure 5.8: The sample is clocked in a 45mT field generated by a permanent magnet.

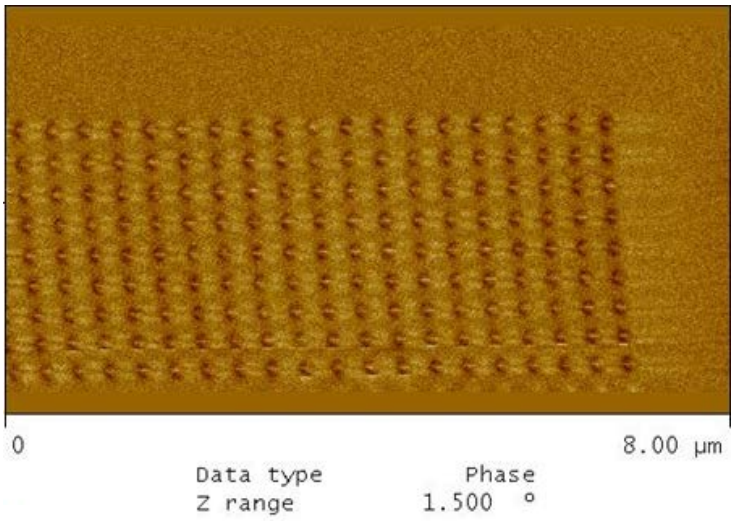

Figure 5.9: MFM image showing tip interference.

the MFM using a MESP-LM probe. The LM probe is the same as the standard probe except it maintains a tip magnetic moment of 0.3e-16Am^2 as compared to the 1e-16Am^2 of the standard probe[41]. The image shown in figure 5.10 was achieved and implied a bias in the clocking field. This same result was obtained after many iterations of the clocking event shown in figure 5.8 and was determined that a different clocking method was needed.

The second clocking technique utilized an electromagnet. An electromagnet was configured to determine what power supply inputs were needed to achieve a magnetic field of

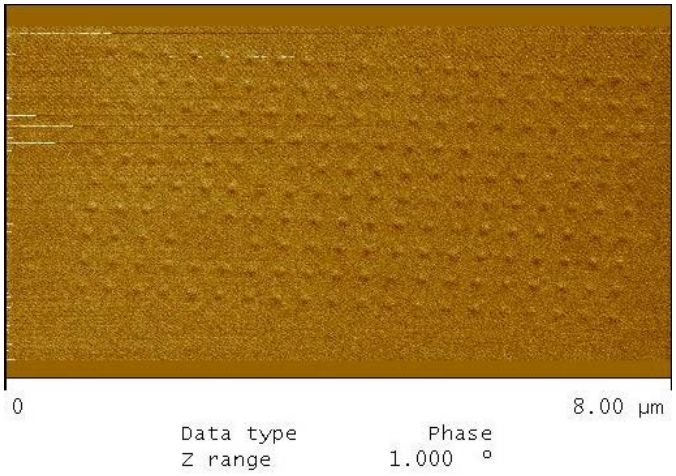

Figure 5.10: MFM image showing alignment of each cell.

45mT. These parameters were noted and the sample was loaded onto the plastic stage between the two pole pieces so that the in-plane hard axis of the array was parallel to the electromagnet field lines. The power supply was engaged to immerse the sample in a 45mT field for 10

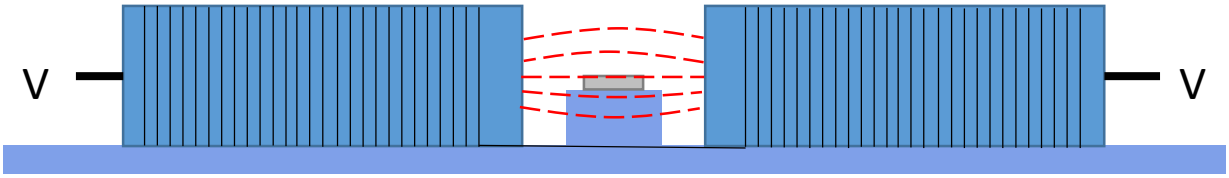

Figure 5.11: The sample is clocked in a 45mT field generated by an electromagnet.

seconds, then the power supply turned off. The setup is shown in figure 5.11. The sample was then imaged in the MFM using the MESP-LM probe. The image shown in figure 5.12 was achieved after many iterations of the electromagnet clocking technique and it was determined that a different clocking method was needed.

A Helmholtz coil was considered for a third clocking technique. Helmholtz coils are a pair of identical coils of diameter R which are spaced R distance apart. The magnetic field produced by this setup is near-uniform [42]. A commercially-available Helmholtz which

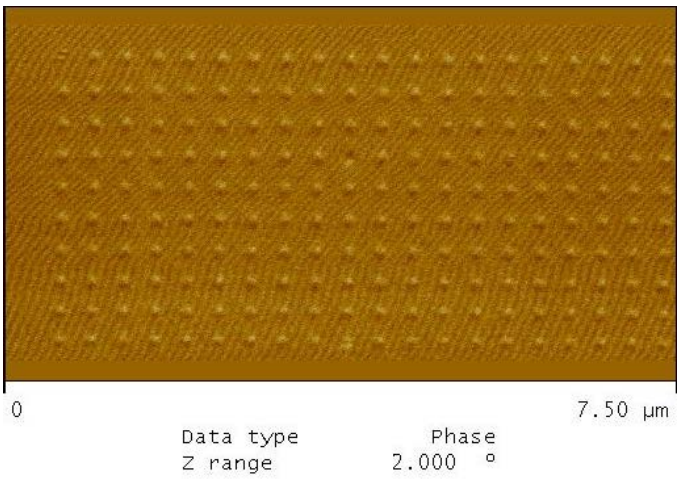

Figure 5.12: MFM image showing tip interference.

produced a 50mT field could not be located, and preliminary calculations for designing a custom Helmholtz proved unrealistic. Therefore, a different clocking method was needed.

The fourth clocking technique involved the use of an AC demagnetization field [43, 44]. The sample was mounted onto a rotating axis and rotated in the magnetic field produced by the electromagnet, as shown in figure 5.13a. The axis of rotation was perpendicular to the applied magnetic field direction and is shown in figure 5.13b. The power supply input was ramped down periodically and its polarity reversed with each step, as shown in figure 5.13c. The clocking field was applied in the in-plane direction and decreased from 80mT to 0mT over an 8 minute span. This AC demagnetization technique is typically utilized for arrays of couple nanomagnets as a way to bring the system to its state of lowest energy. Using this technique with an array of decoupled nanomagnets essentially assigns each cell a random state and thereby induces

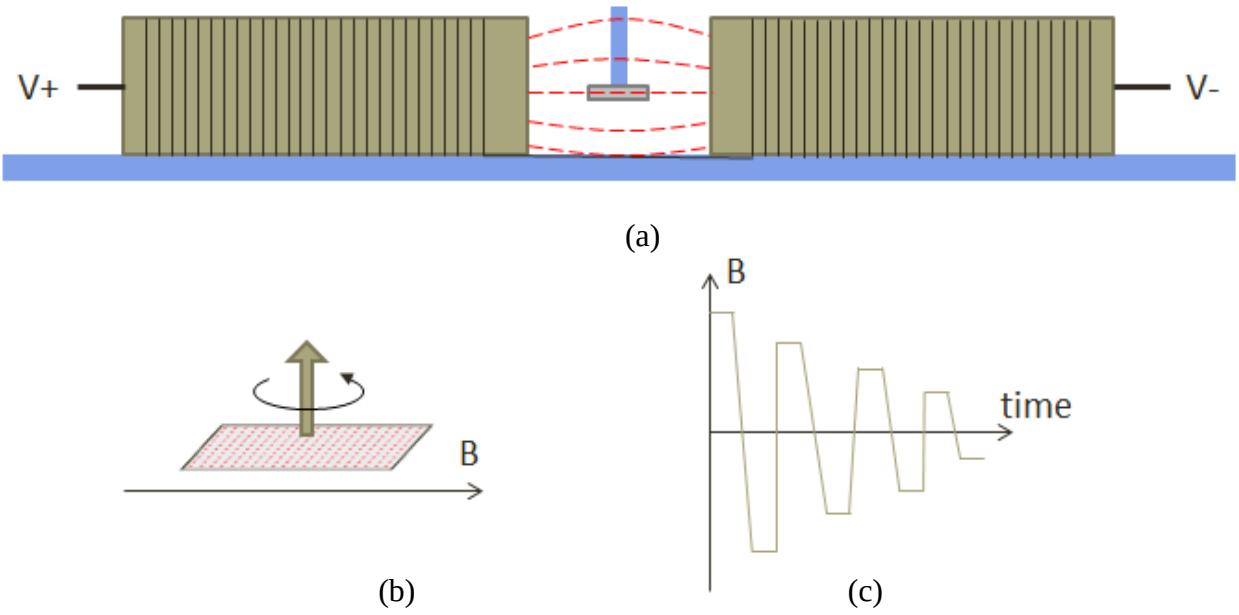

Figure 5.13: (a) Shows the sample suspended from a rotating axis inside the electromagnet-produced magnetic field. (b) Shows the axis of rotation with respect to an array of nanomagnets and the appled field, and (c) shows the applied magnetic field.

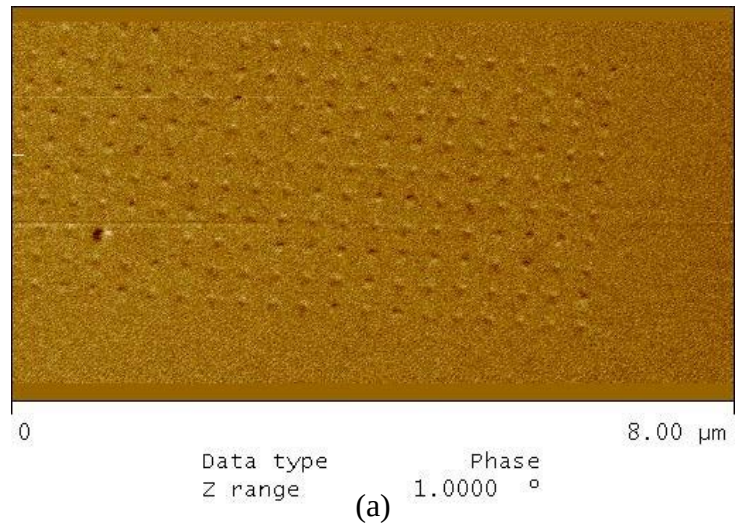

(a)

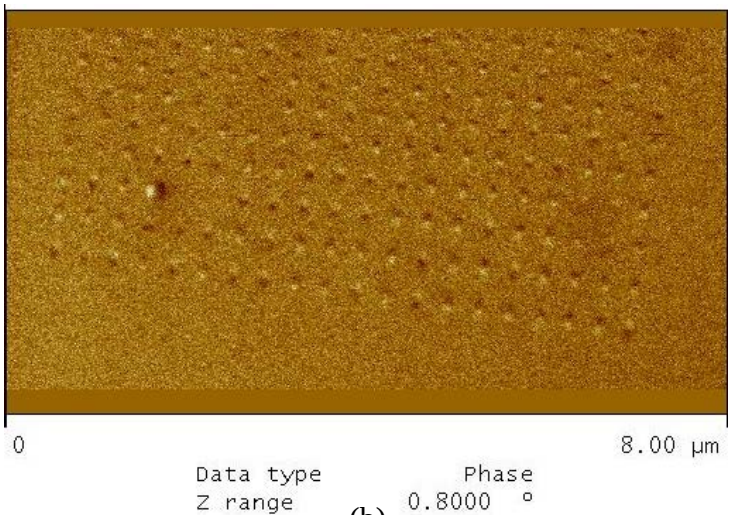

(b)

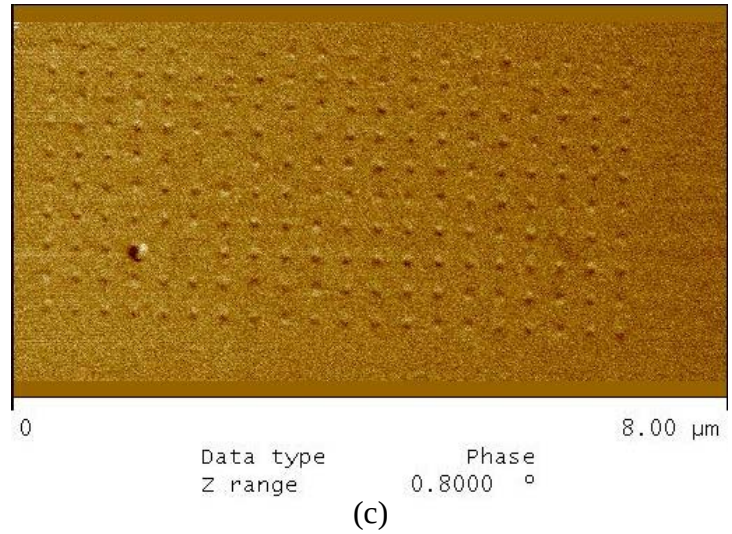

(c)

Figure 5.14: Three MFM images of different AC demagnetization clocking events.

randomness across the entire array. Figure 5.14 shows three MFM scans captured after different AC demagnetization clocking events, and tables 5.6-5.8 show the respective MFM scan parameters used for each scan.

Table 5.6: Scan parameters used to obtain MFM image of PUF-1 sample shown in figure 5.14a.

Parameter	Setting
Scan Rate	0.5Hz
Drive Frequency	71.221kHz
Drive Amplitude	3,800mV
Lift Scan Height	35nm

Table 5.7: Scan parameters used to obtain MFM image of PUF-1 sample shown in figure 5.14b.

Parameter	Setting
Scan Rate	0.5Hz
Drive Frequency	71.183kHz
Drive Amplitude	836.14mV
Lift Scan Height	35nm

Table 5.8: Scan parameters used to obtain MFM image of PUF-1 sample shown in figure 5.14c.

Parameter	Setting
Scan Rate	0.5Hz
Drive Frequency	72.227kHz
Drive Amplitude	4,000mV
Lift Scan Height	35nm

A height image of the PUF-1 array is shown in figure 5.15. It was measured at approximately 13.5nm and though this was thicker than the targeted 10nm thickness, it was still acceptable.

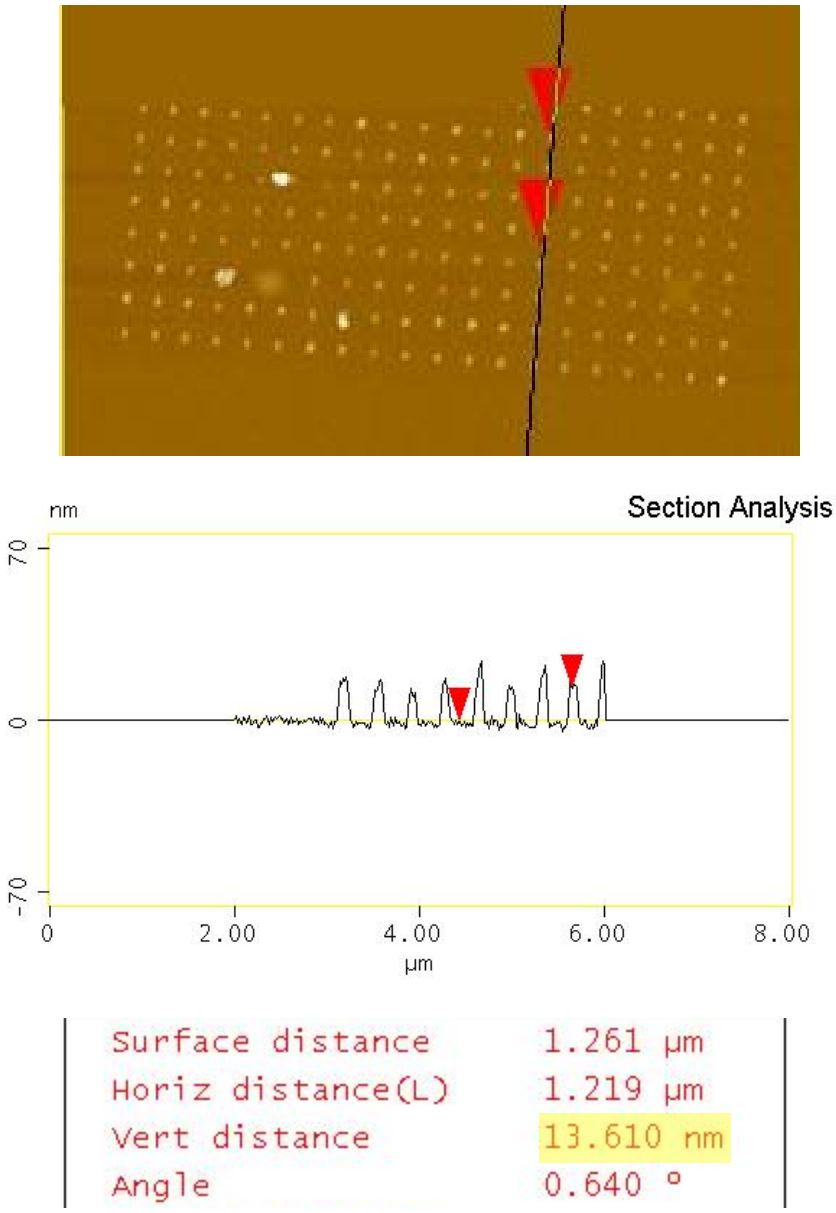

Figure 5.15: A height image of the PUF-1 sample.

Future work involves optimizing the clocking technique so that an array which maintains the same state of randomness propagates through clocking events. However, the experimental

display of entropy in an array of decoupled nanomagnets provided supportive data for a journal paper [30], conference presentation [45], and a patent [46].

5.2.2 PUF-2

The objective of the SEM characterization of the PUF-2 sample was to identify an array of elliptical nanomagnets and an array of dimensionally-equal rectangular nanomagnets that maintained nearly-identical dimensions as their respective CAD arrays. SEM images were then captured of each individual nanomagnet within each array. These images were sent to other members of the lab to be used in simulation experiments of the PUF device. MFM characterization was not performed on these samples.

Since the samples were not being used for MFM analysis, proper inter-feature spacings which would eliminate neighbor coupling were not critical from an experimental standpoint. However, arrays demonstrating proper inter-feature spacing were still identified and imaged so that the most accurate and realistic cells would be simulated. Table 5.9 shows he primary beam and column parameters used during characterization of the PUF-2 sample. Figure 5.16 shows images taken from the PUF-2 elliptical array and figure 5.17 shows images taken from the PUF-2 rectangular array.

Table 5.9: Primary beam and column parameters during SEM characterization of PUF-2.

Parameter	Setting
Accelerating Voltage	30kV
Working Distance	~9.5mm
Landing Current	~24pA
Objective Lens	Lower (Normal)

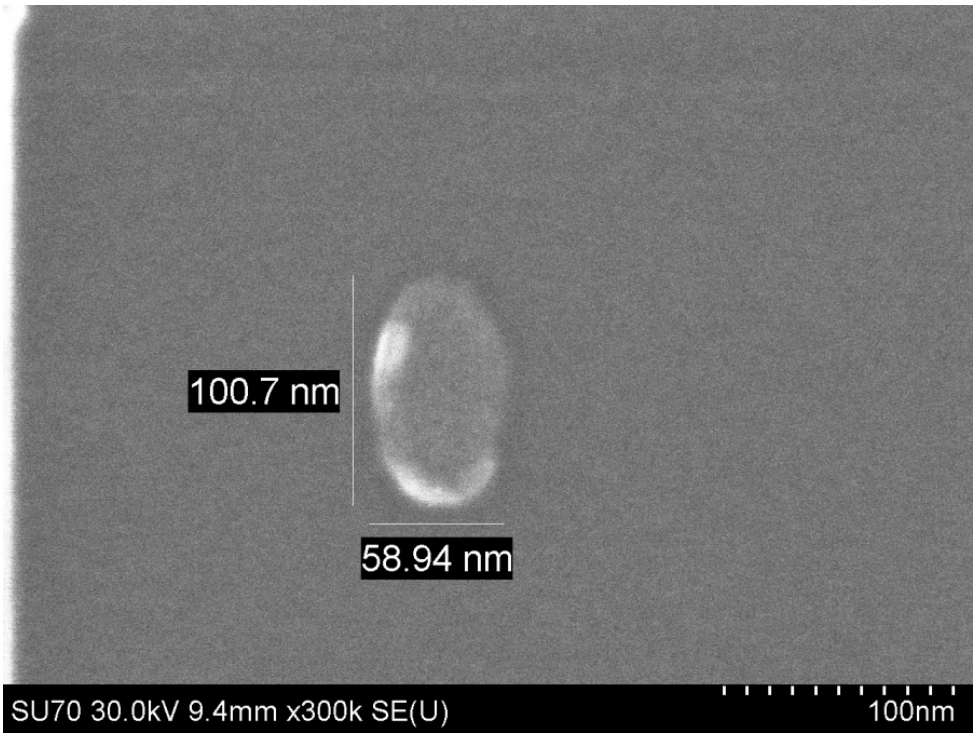

(a)

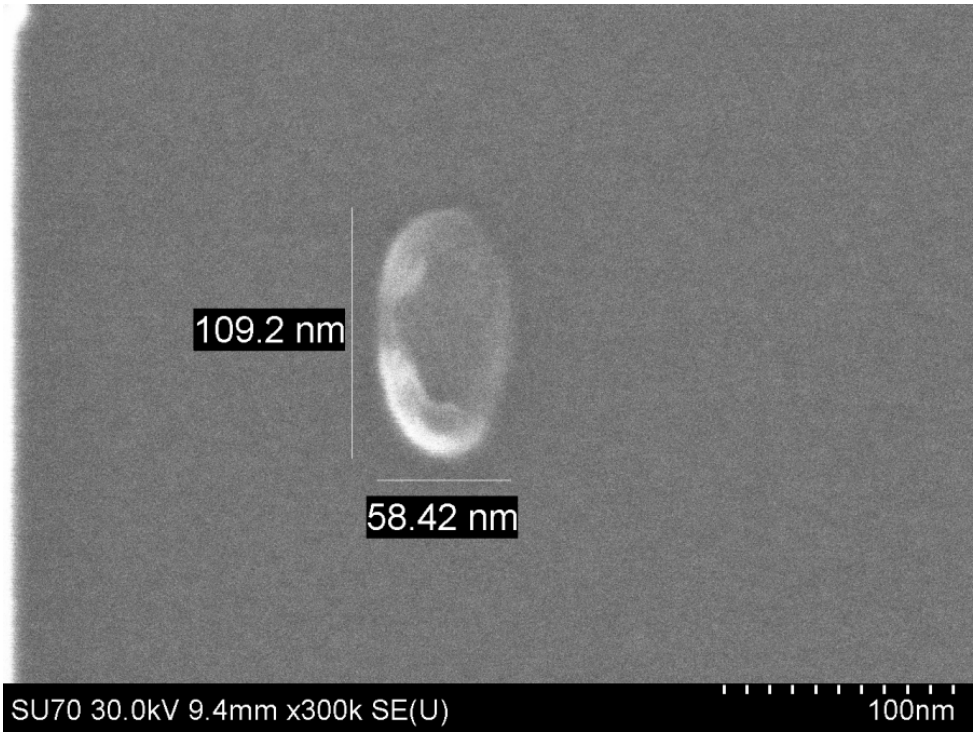

(b)

Figure 5.16: Two elliptical nanomagnets from the PUF-2 elliptical array.

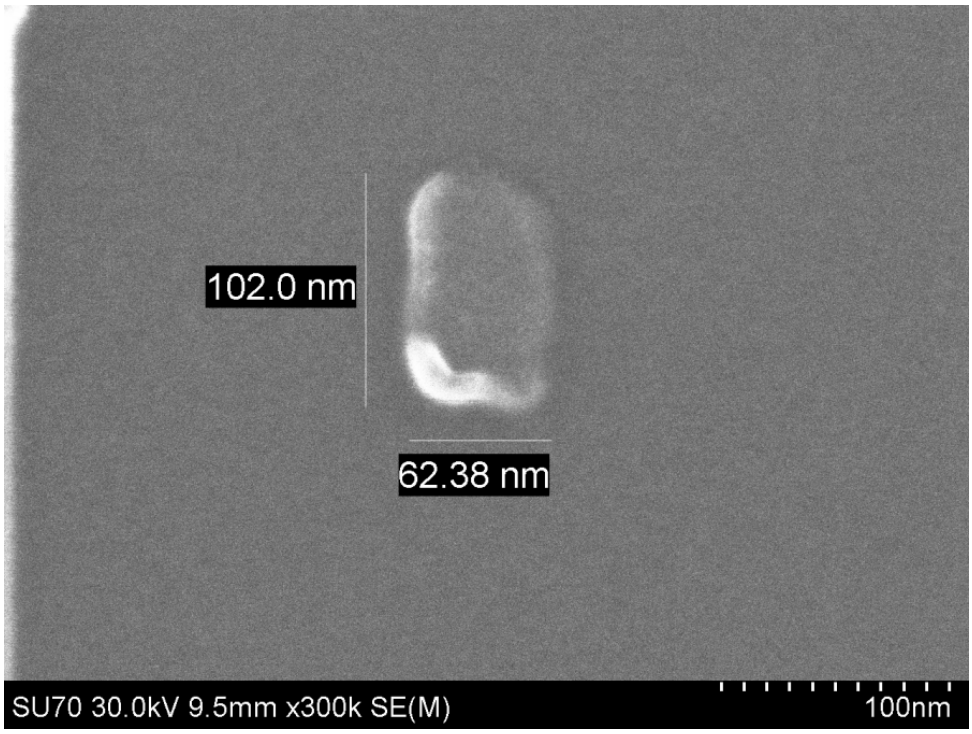

(a)

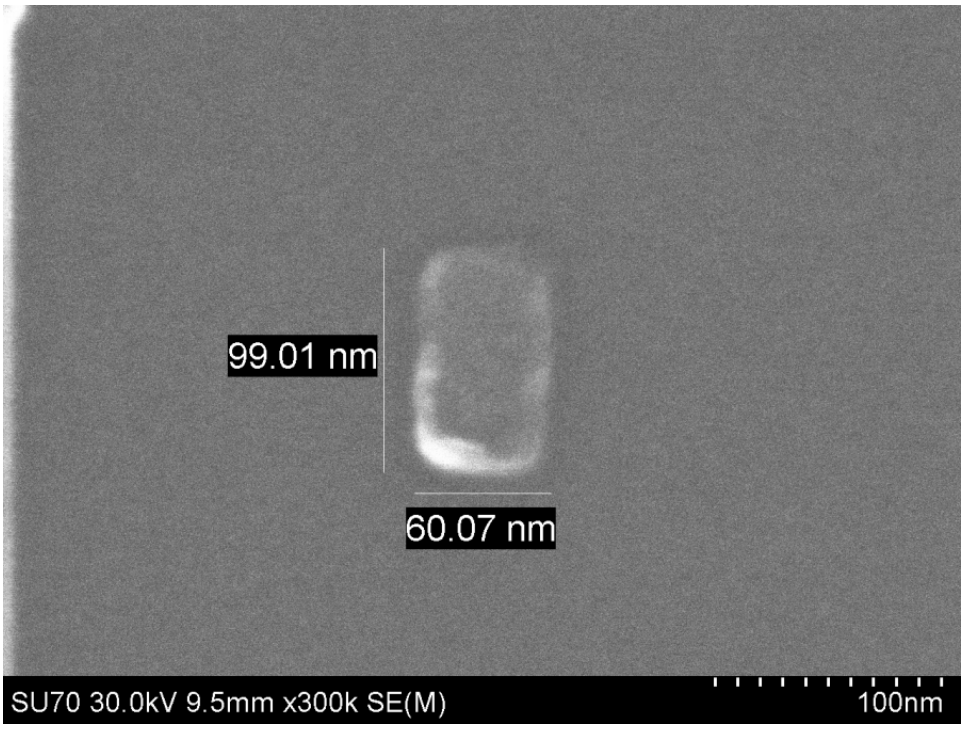

(b)

Figure 5.17: Two rectangular nanomagnets from the PUF-2 elliptical array.

5.3 Vision

The objective of the SEM characterization of the Vision sample was to identify which exposure dose produced the most optimal group of arrays. The objective of the MFM characterization was to obtain an image of the magnetic state of the system, specifically an image that contains single domain nanodiscs and vortex domain nanodiscs.

Proper dosing was critical in the Vision samples. Each nanodisc within the pattern had a diameter of 145nm and a nearest neighbor spacing of 20nm. The center of each array contained a dense concentration of nanodiscs and a slight overdose would cause these discs to bleed together because of the proximity effect. Overdosed samples were generally identifiable by this bleeding effect and an example is shown in figure 5.18. Arrays not displaying this bleeding were measured to determine which pattern maintained proper dimensions and spacings as compared to the CAD pattern. Properly dosed patterns are shown in figure 5.19.

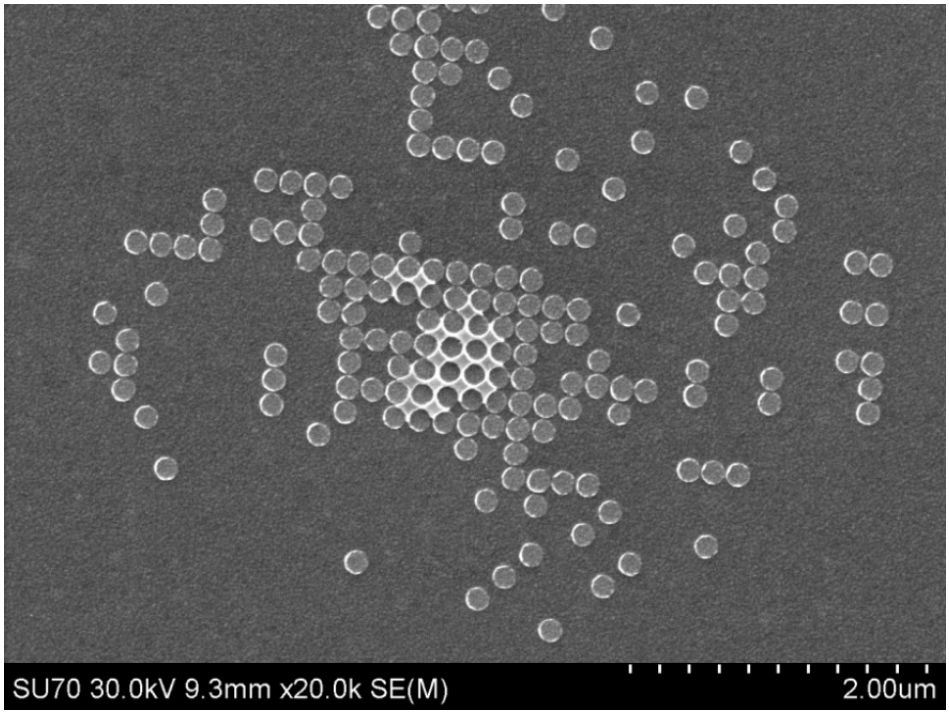

Figure 5.18: A Vision pattern showing bleeding from exposure overdose.

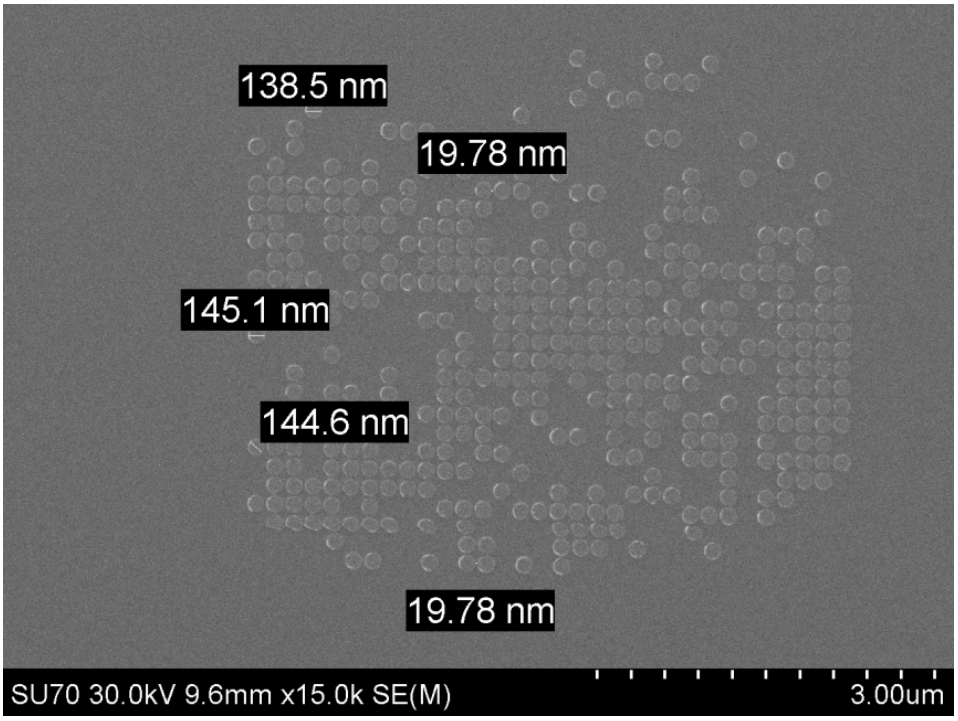

(a)

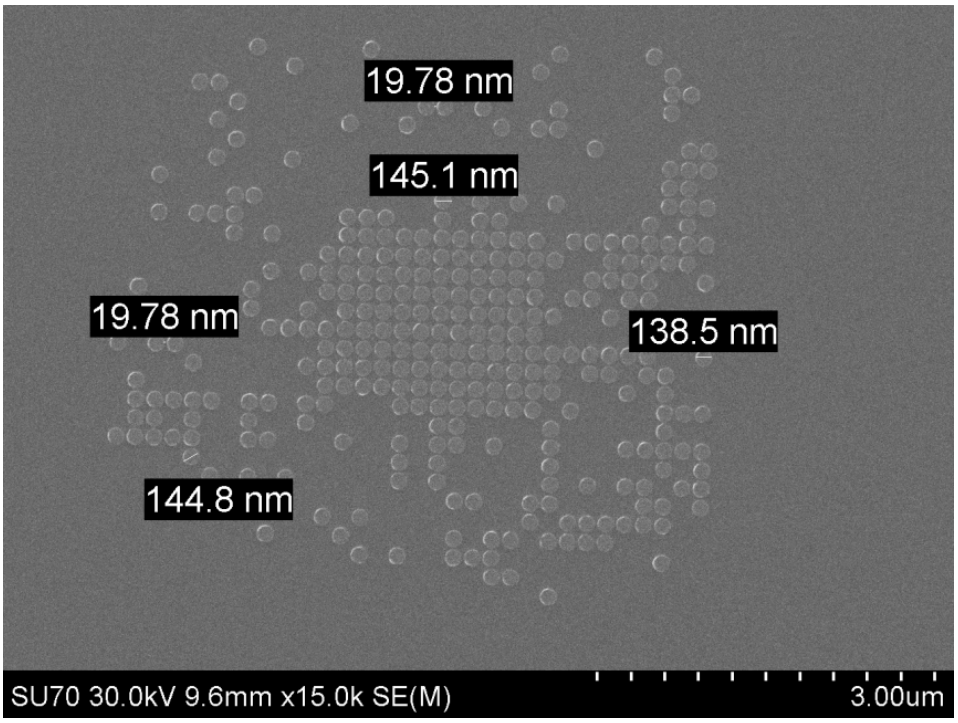

(b)

Figure 5.19: Two Vision patterns of proper exposure dose and dimensions.

The Vision pattern was then imaged with an MESP-LM tip. The sample was clocked in-plane with an 80mT field for 3 seconds using a permanent magnet. Since the nanodiscs are circular there is no in-plane hard axis, so the array was rather arbitrarily clocked in-plane. Figure 5.20 shows an AFM height scan of the Vision sample and shows that the Vision height is approximately 12.5nm. Figures 5.21-25 show an MFM image of each of the five Vision patterns. Tables 5.10-5.14 show the respective MFM scan parameters used for each MFM image.

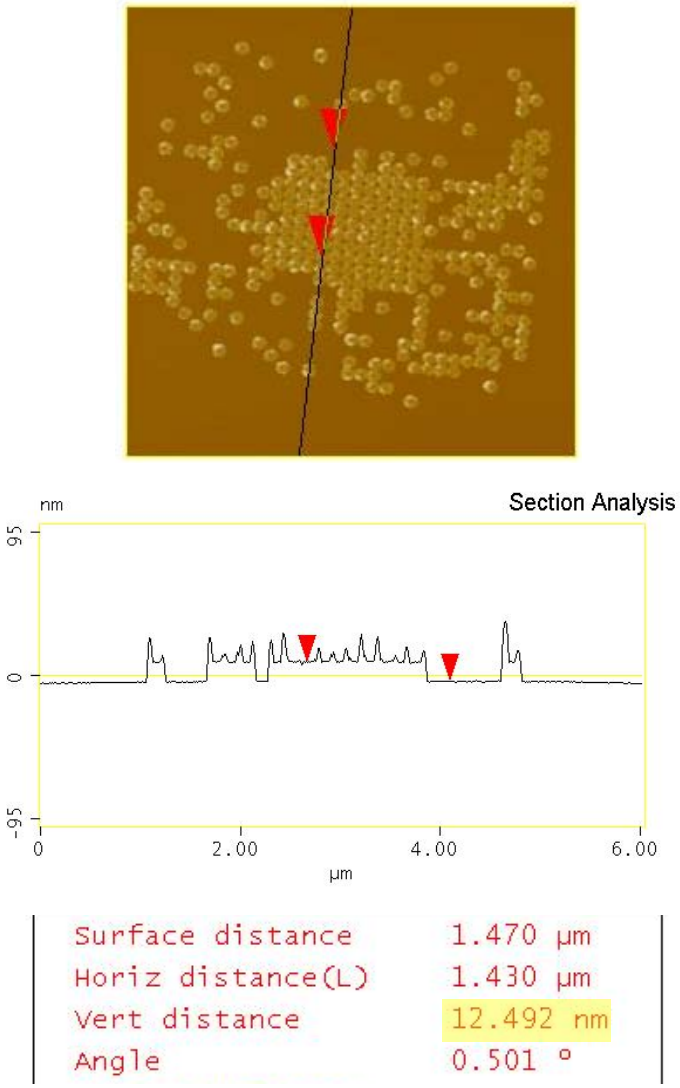

Figure 5.20: AFM height image of Vision sample.

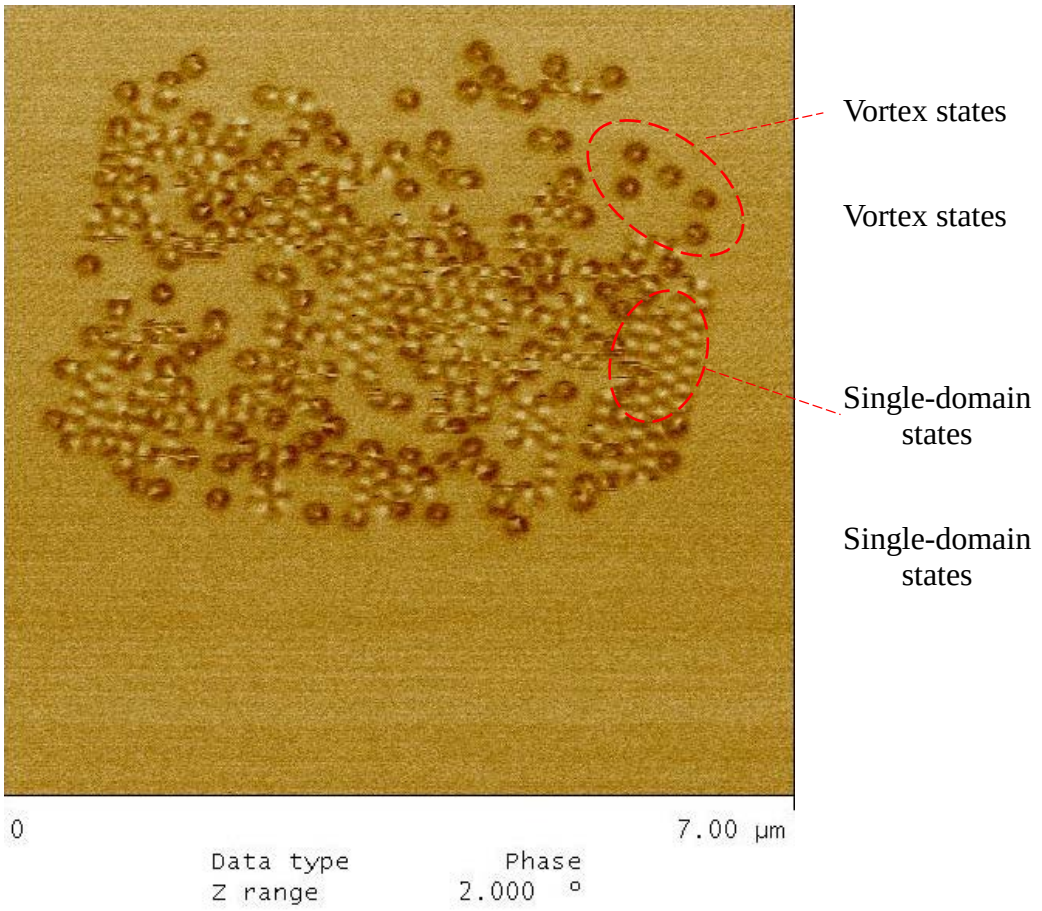

Figure 5.21: MFM of first Vision pattern.

Table 5.10: Scan parameters used to obtain MFM image of first Vision pattern.

Parameter	Setting
Scan Rate	0.5Hz
Drive Frequency	72.001kHz
Drive Amplitude	1,600mV
Lift Scan Height	35nm

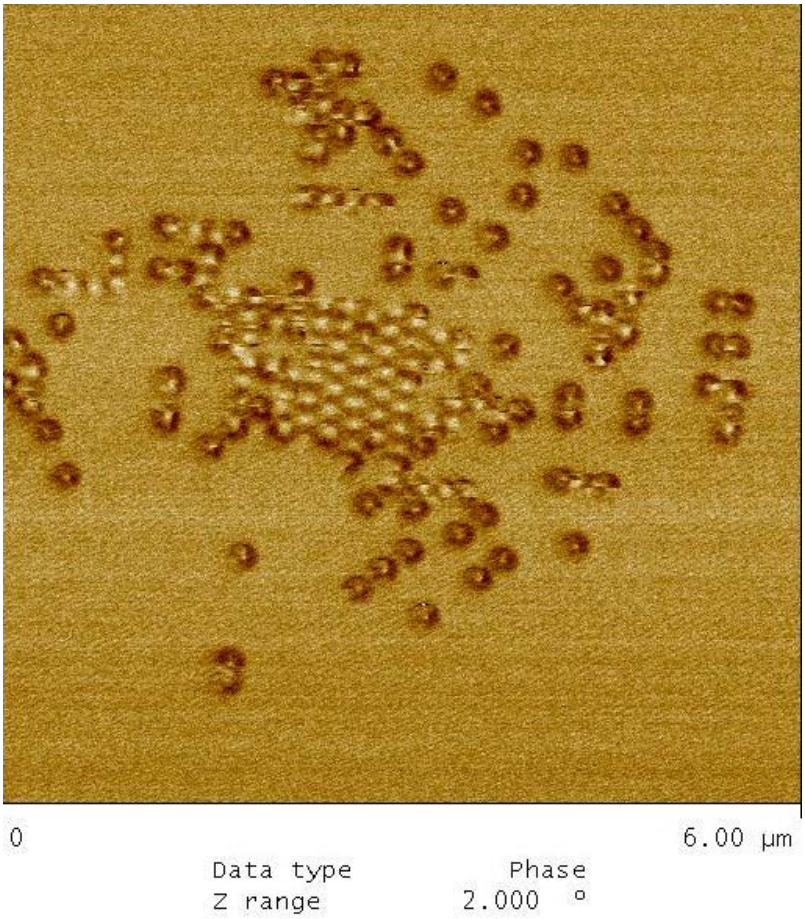

Figure 5.22: MFM of second Vision pattern.

Table 5.11: Scan parameters used to obtain MFM image of second Vision pattern.

Parameter	Setting
Scan Rate	0.5Hz
Drive Frequency	73.145kHz
Drive Amplitude	1,200mV
Lift Scan Height	35nm

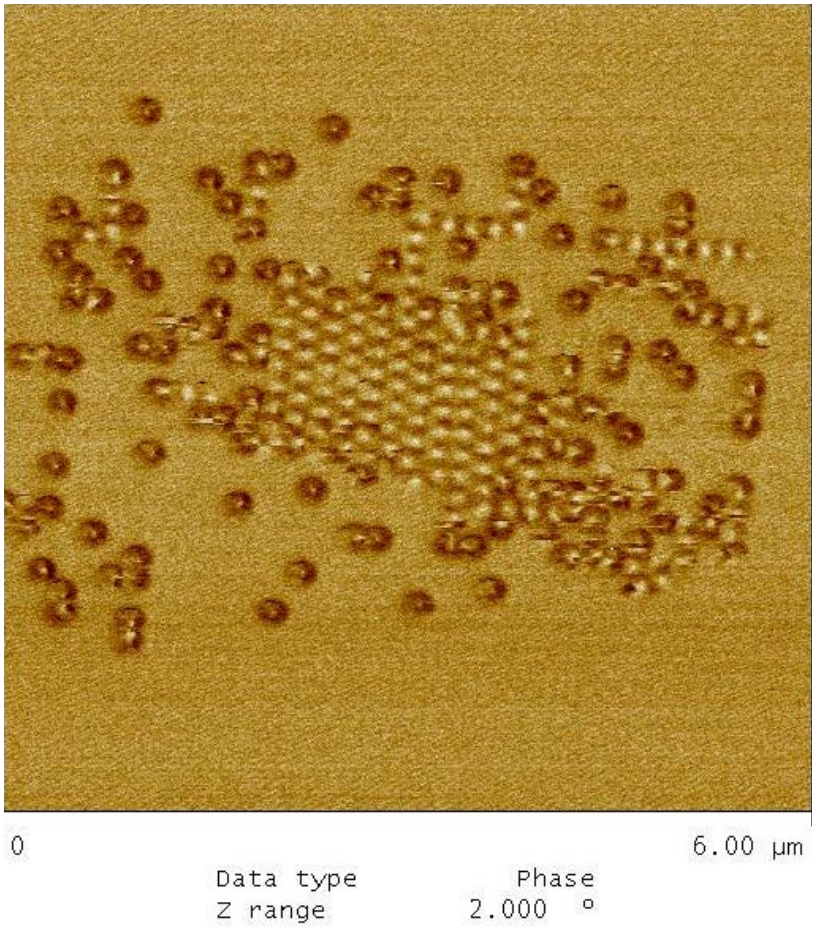

Figure 5.23: MFM of third Vision pattern.

Table 5.12: Scan parameters used to obtain MFM image of third Vision pattern.

Parameter	Setting
Scan Rate	0.5Hz
Drive Frequency	73.145kHz
Drive Amplitude	1,300mV
Lift Scan Height	35nm

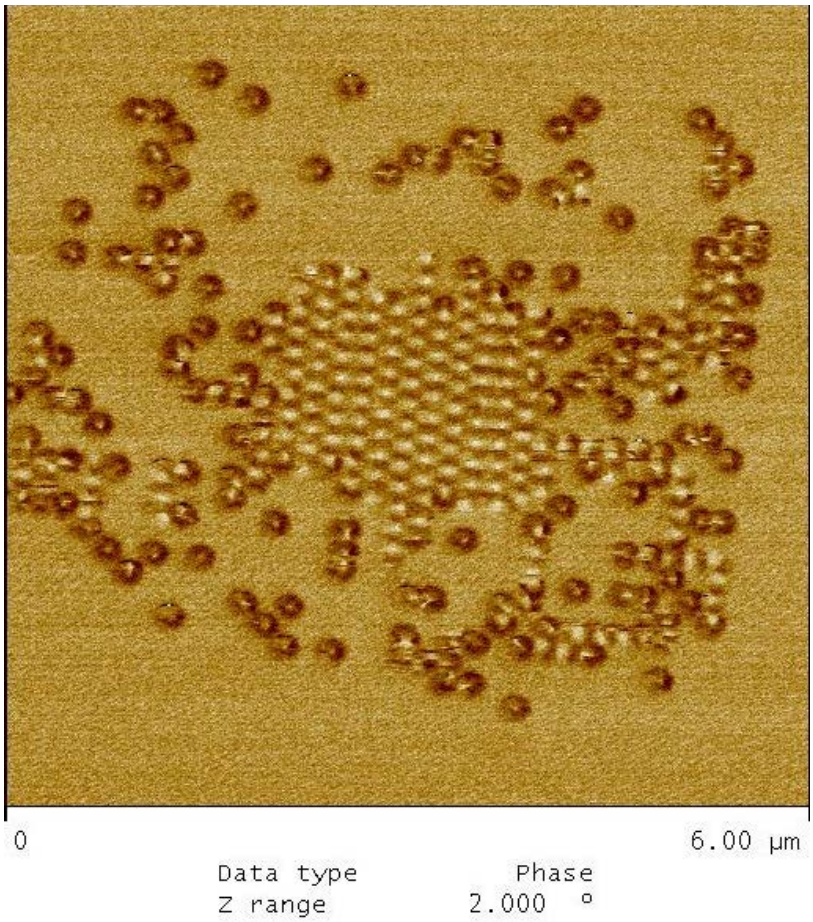

Figure 5.24: MFM of fourth Vision pattern.

Table 5.13: Scan parameters used to obtain MFM image of fourth Vision pattern.

Parameter	Setting
Scan Rate	0.5Hz
Drive Frequency	73.145kHz
Drive Amplitude	1,300mV
Lift Scan Height	35nm

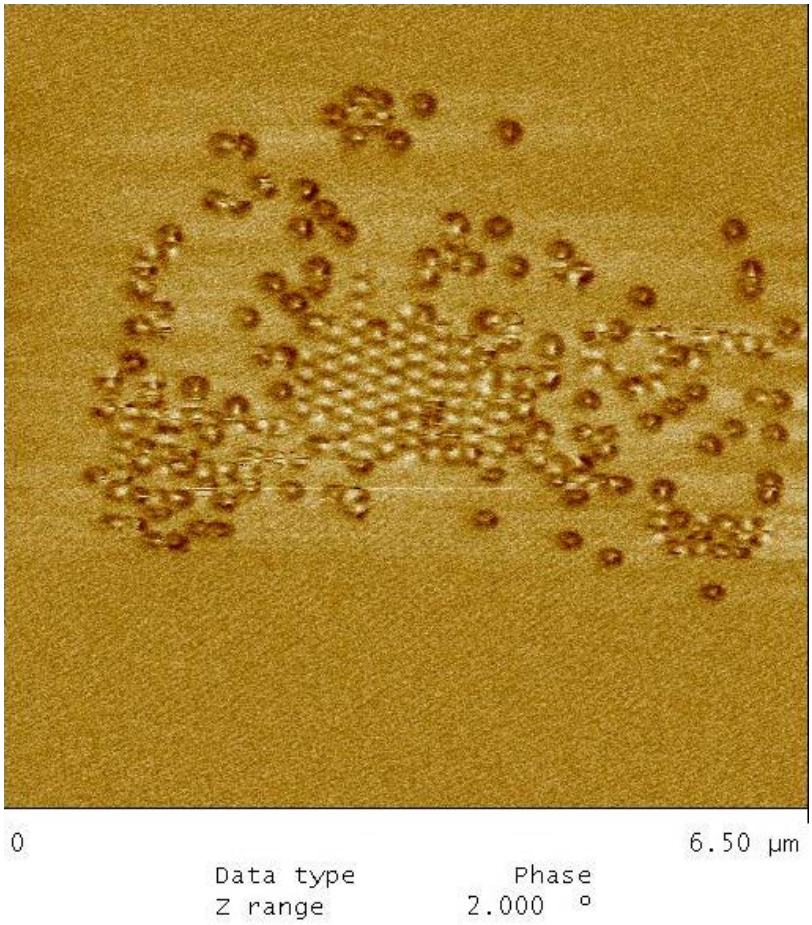

Figure 5.25: MFM of fifth Vision pattern.

Table 5.14: Scan parameters used to obtain MFM image of fifth Vision pattern.

Parameter	Setting
Scan Rate	0.5Hz
Drive Frequency	73.145kHz
Drive Amplitude	1,200mV
Lift Scan Height	35nm

Chapter 6: Conclusion

Four samples from three different sample groups were fabricated and characterized in this thesis. All samples contained magnetic nanostructures, but each sample group contained structures of different types. The DWM sample contained magnetic nanowires that were fabricated and characterized as a proof-of-ability demonstration to a lab group from another university as a potential collaboration effort. The PUF samples contained arrays of decoupled nanomagnets who maintained a magnetic easy axis as a result of shape anisotropy. A clocking field was applied to an array to demagnetize the system and produce a random signature of domain states. This work provided experimental support for a conference presentation [45], a journal paper under review [30], and a filed patent [46]. The Vision samples contained unique patterns of specifically-placed magnetic nanodiscs that would interact with each other to produce magnetic states of a single domain nature or a vortex nature. This work was completed to provide more experimental data points to verify and optimize performance of this novel quadratic optimization device.

Future work would begin with optimizing the clocking technique for the PUF samples. This would allow consistent intrinsic randomness to be displayed throughout the PUF arrays after each clocking event instead of the randomly-induced randomness observed. Also, the samples would be integrated into multilayer structures in order to achieve and study a more realistic device. The work performed in this thesis, however, provided groundwork for an

experimental PUF design which displayed entropy as well as numerous more data points for the continued focus on the Vision problem.

References

[1] G. H. Bernstein, A. Imre, V. Metlushko, A. Orlov, L. Zhou, L. Ji, *et al.*, "Magnetic QCA systems," *Microelectronics Journal,* vol. 36, pp. 619-624, 2005.

[2] R. Cowburn and M. Welland, "Room temperature magnetic quantum cellular automata," *Science,* vol. 287, pp. 1466-1468, 2000.

[3] G. Csaba, *Computing with field-coupled nanomagnets*, 2003.

[4] J. F. Pulecio, "Field-Coupled Nano-Magnetic Logic Systems," University of South Florida, 2010.

[5] D. Karunaratne and S. Adviser-Bhanja, *Nano-magnetic devices for computation*: University of South Florida, 2013.

[6] ARTE, "SEM schematic," ed. Wikimedia Commons, 2007, p. Diagram of a scanning electron microscope with English captions.

[7] R. Cowburn, "Magnetic nanodots for device applications," *Journal of magnetism and magnetic materials,* vol. 242, pp. 505-511, 2002.

[8] D. Karunaratne and S. Bhanja, "Study of single layer and multilayer nano-magnetic logic architectures," *Journal of Applied Physics,* vol. 111, p. 07A928, 2012.

[9] S. Sarkar and S. Bhanja, "Direct quadratic minimization using magnetic field-based computing," in *Design and Test of Nano Devices, Circuits and Systems, 2008 IEEE International Workshop on*, 2008, pp. 31-34.

[10] J. Orloff, *Handbook of Charged Particle Optics*: Taylor & Francis, 1997.

[11] A. Khursheed, *Scanning Electron Microscope Optics and Spectrometers*: World Scientific, 2011.

[12] D. C. Joy, "Beam interactions, contrast and resolution in the SEM," *Journal of Microscopy,* vol. 136, pp. 241-258, 1984.

[13] "Scanning Electron Microscope A to Z: Basic Knowledge for Using the SEM," JEOL, 2009.

[14] F. Krumeick, "Properties of electrons, their interactions with matter and applications in electron microscopy," *Laboratory of Inorganic Chemistry, disponível em http://www. microscopy. ethz. ch/downloads/Interactions. pdf, consultado em*, pp. 3-08, 2011.

[15] "Invitation to the SEM World," JEOL.

[16] J. C. Nabity, *Nanometer Pattern Generation System User's Manual*, NPGS v8 and v9 ed., 2002.

[17] R. G. Dominique Drouin, Pierre Hovongton, "Casino: monte CArlo SImulation of electroN trajectory in sOlids," vol. 2.48, ed. University of Sherbrooke, 2011.

[18] K. Koshelev, M. A. Mohammad, T. Fito, K. L. Westra, S. K. Dew, and M. Stepanova, "Comparison between ZEP and PMMA resists for nanoscale electron beam lithography experimentally and by numerical modeling," *Journal of Vacuum Science & Technology B*, vol. 29, p. 06F306, 2011.

[19] R. Wiesendanger, *Scanning Probe Microscopy and Spectroscopy: Methods and Applications*: Cambridge University Press, 1994.

[20] *TESP*. Bruker. http://www.brukerafmprobes.com/Product.aspx?ProductID=3394

[21] D. Brandon and W. D. Kaplan, *Microstructural Characterization of Materials*: Wiley, 2013.

[22] W. R. Bowen and N. Hilal, *Atomic Force Microscopy in Process Engineering: An Introduction to AFM for Improved Processes and Products*: Elsevier Science, 2009.

[23] Y. Roiter and S. Minko, "AFM single molecule experiments at the solid-liquid interface: in situ conformation of adsorbed flexible polyelectrolyte chains," *Journal of the American Chemical Society*, vol. 127, pp. 15688-15689, 2005.

[24] *Dimension 3100 AFM Instruction Manual*, Version 4.31ce ed.: Digital Instruments, Inc., 1997.

[25] *NanoScope Command Reference Manual*, Version 5.12 rev B ed.: Digital Instruments / Veeco Metrology Group, Inc., 2001.

[26] P. I. Bonyhard, Y.-S. Chen, and J. L. Smith, "Magnetic bubble memory organization," ed: Google Patents, 1977.

[27] S. S. Parkin, M. Hayashi, and L. Thomas, "Magnetic domain-wall racetrack memory," *Science*, vol. 320, pp. 190-194, 2008.

[28] M. Hayashi, L. Thomas, R. Moriya, C. Rettner, and S. S. Parkin, "Current-controlled magnetic domain-wall nanowire shift register," *Science*, vol. 320, pp. 209-211, 2008.

[29] M. Roel, "Physically unclonable functions: Constructions, properties and applications," Dissertation, University of KU Leuven, 2012.

[30] Jayita Das, Kevin Scott, Srinath Rajaram, Drew Burgett, Sanjukta Bhanja., "MRAM PUF: A Novel Geometry Based Magnetic PUF With Integrated CMOS," *IEEE Transactions on Nanotechnology,* 2014.

[31] J. Pulecio, S. Bhanja, and S. Sarkar, "An experimental demonstration of the viability of energy minimizing computing using nano-magnets," in *Nanotechnology (IEEE-NANO), 2011 11th IEEE Conference on*, 2011, pp. 1038-1042.

[32] K. L. Boyer and S. Sarkar, "GUEST EDITORS'INTRODUCTION: Perceptual Organization in Computer Vision: Status, Challenges, and Potential," *Computer Vision and Image Understanding*, vol. 76, pp. 1-5, 1999.

[33] R. Cowburn, D. Koltsov, A. Adeyeye, M. Welland, and D. Tricker, "Single-domain circular nanomagnets," *Physical Review Letters,* vol. 83, p. 1042, 1999.

[34] C. Vieu, F. Carcenac, A. Pépin, Y. Chen, M. Mejias, A. Lebib, *et al.*, "Electron beam lithography: resolution limits and applications," *Applied Surface Science*, vol. 164, pp. 111-117, 9/1/ 2000.

[35] *PMMA Data Sheet*. MicroChem. http://microchem.com/pdf/PMMA_Data_Sheet.pdf

[36] J. C. Nabity. (2005). *NPGS: Contamination Spots.* Available: http://www.jcnabity.com/c_spot1.htm

[37] A. Kokkinis, E. Valamontes, D. Goustouridis, T. Ganetsos, K. Beltsios, and I. Raptis, "Molecular weight and processing effects on the dissolution properties of thin poly (methyl methacrylate) films," *Microelectronic Engineering*, vol. 85, pp. 93-99, 2008.

[38] L. Masaro and X. X. Zhu, "Physical models of diffusion for polymer solutions, gels and solids," *Progress in Polymer Science*, vol. 24, pp. 731-775, 8// 1999.

[39] M. A. Mohammad, M. Muhammad, S. K. Dew, and M. Stepanova, *Fundamentals of electron beam exposure and development*: Springer, 2012.

[40] H. Arnold and G. Elmen, "Permalloy, a new magnetic material of very high permeability," *Bell System Technical Journal*, vol. 2, pp. 101-111, 1923.

[41] *MESP-LM*. Bruker. http://www.brukerafmprobes.com/p-3315-mesp-lm.aspx

[42] E. L. Bronaugh, "Helmholtz coils for calibration of probes and sensors: limits of magnetic field accuracy and uniformity," in *Electromagnetic Compatibility, 1995. Symposium Record., 1995 IEEE International Symposium on*, 1995, pp. 72-76.

[43] R. Wang, J. Li, W. McConville, C. Nisoli, X. Ke, J. Freeland, *et al.*, "Demagnetization protocols for frustrated interacting nanomagnet arrays," *Journal of applied physics,* vol. 101, p. 09J104, 2007.

[44] X. Ke, J. Li, C. Nisoli, P. E. Lammert, W. McConville, R. Wang, *et al.*, "Energy minimization and ac demagnetization in a nanomagnet array," *Physical review letters,* vol. 101, p. 037205, 2008.

[45] Jayita Das, Kevin Scott, Drew Burgett, Srinath Rajaram, Sanjukta Bhanja., "A Novel Geometry Based MRAM PUF," in *IEEE Nano '14 Conference*, Toronto, Canada, 2014.

[46] Jayita Das, Kevin P. Scott, Drew H. Burgett, Srinath Rajaram, Sanjukta Bhanja., "Geometry Based Magnetic PUF," 2014.

Appendices

Appendix A: Copyright Permissions for General Use of Published Information

Copyright | Fair Use

One of the rights accorded to the owner of copyright is the right to reproduce or to authorize others to reproduce the work in copies or phonorecords. This right is subject to certain limitations found in sections 107 through 118 of the copyright law (title 17, U. S. Code). One of the more important limitations is the doctrine of "fair use." The doctrine of fair use has developed through a substantial number of court decisions over the years and has been codified in section 107 of the copyright law.

Section 107 contains a list of the various purposes for which the reproduction of a particular work may be considered fair, such as criticism, comment, news reporting, teaching, scholarship, and research. Section 107 also sets out four factors to be considered in determining whether or not a particular use is fair.

1. The purpose and character of the use, including whether such use is of commercial nature or is for nonprofit educational purposes
2. The nature of the copyrighted work
3. The amount and substantiality of the portion used in relation to the copyrighted work as a whole
4. The effect of the use upon the potential market for, or value of, the copyrighted work

The distinction between what is fair use and what is infringement in a particular case will not always be clear or easily defined. There is no specific number of words, lines, or notes that may safely be taken without permission. Acknowledging the source of the copyrighted material does not substitute for obtaining permission.

The 1961 *Report of the Register of Copyrights on the General Revision of the U.S. Copyright Law* cites examples of activities that courts have regarded as fair use: "quotation of excerpts in a review or criticism for purposes of illustration or comment; quotation of short passages in a scholarly or technical work, for illustration or clarification of the author's observations; use in a parody of some of the content of the work parodied; summary of an address or article, with brief quotations, in a news report; reproduction by a library of a portion of a work to replace part of a damaged copy; reproduction by a teacher or student of a small part of a work to illustrate a lesson; reproduction of a work in legislative or judicial proceedings or reports; incidental and fortuitous reproduction, in a newsreel or broadcast, of a work located in the scene of an event being reported."

Copyright protects the particular way authors have expressed themselves. It does not extend to any ideas, systems, or factual information conveyed in a work.

The safest course is to get permission from the copyright owner before using copyrighted material. The Copyright Office cannot give this permission.

When it is impracticable to obtain permission, you should consider avoiding the use of copyrighted material unless you are confident that the doctrine of fair use would apply to the situation. The Copyright Office can neither determine whether a particular use may be considered fair nor advise on possible copyright violations. If there is any doubt, it is advisable to consult an attorney.

FL-102, Reviewed June 2012

U.S. Copyright Office
101 Independence Avenue SE
Washington, DC 20559-6000
(202) 707-3000

Appendix B: Copyright Permissions for Use of Figure 2.1

I, the copyright holder of this work, hereby publish it under the following licenses:

This file is licensed under the Creative Commons Attribution-Share Alike 1.0 Generic license.

You are free:

- **to share** – to copy, distribute and transmit the work
- **to remix** – to adapt the work

Under the following conditions:

- **attribution** – You must attribute the work in the manner specified by the author or licensor (but not in any way that suggests that they endorse you or your use of the work).
- **share alike** – If you alter, transform, or build upon this work, you may distribute the resulting work only under the same or similar license to this one.

This file is licensed under the Creative Commons Attribution-Share Alike 3.0 Unported license.

You are free:

- **to share** – to copy, distribute and transmit the work
- **to remix** – to adapt the work

Under the following conditions:

- **attribution** – You must attribute the work in the manner specified by the author or licensor (but not in any way that suggests that they endorse you or your use of the work).
- **share alike** – If you alter, transform, or build upon this work, you may distribute the resulting work only under the same or similar license to this one.

This licensing tag was added to this file as part of the GFDL licensing update.

Permission is granted to copy, distribute and/or modify this document under the terms of the **GNU Free Documentation License**, Version 1.2 or any later version published by the Free Software Foundation; with no Invariant Sections, no Front-Cover Texts, and no Back-Cover Texts. A copy of the license is included in the section entitled *GNU Free Documentation License*.

You may select the license of your choice.